2009-07-07

Evans Function Computation

Blake H. Barker
Brigham Young University - Provo

EVANS FUNCTION COMPUTATION

by

Blake Barker

A thesis submitted to the faculty of

Brigham Young University

in partial fulfillment of the requirements for the degree of

Master of Science

Department of Mathematics

Brigham Young University

August 2009

BRIGHAM YOUNG UNIVERSITY

GRADUATE COMMITTEE APPROVAL

of a thesis submitted by

Blake Barker

This thesis has been read by each of member of the following graduate committee and by majority vote has been found to be satisfactory.

_____   _____
Date   Jeffrey Humpherys, Chair

_____   _____
Date   Kening Lu

_____   _____
Date   Shue-Sum Chow

ABSTRACT

Evans Function Computation

Blake Barker

Department of Mathematics

Master of Science

In this thesis, we review the stability problem for traveling waves and discuss the Evans function, an emerging tool in the stability analysis of traveling waves. We describe some recent developments in the numerical computation of the Evans function and discuss STABLAB, an interactive MATLAB based tool box that we developed. In addition, we verify the Evans function for shock layers in Burgers equation and the p-system with and without capillarity, as well as pulses in the generalized Kortweg-de Vries (gKdV) equation. We conduct a new study of parallel shock layers in isentropic magnetohydrodynamics (MHD) obtaining results consistent with stability.

TABLE OF CONTENTS

LIST OF TABLES

LIST OF FIGURES

Chapter 1. Introduction

In this thesis we study the stability of traveling waves in viscous compressible fluid dynamics. Traveling waves occur in detonations in a reactive gas, as shallow water waves, as shock layers in a viscous plasma, and in many other observable natural phenomena. Small disturbances to these traveling waves may propagate causing the state of the system to alter, e.g. to bifurcate. Alternatively, the state of the system may persist for all time assuming the disturbance is small enough. For a dissipative traveling wave, stability means the shape of the wave is preserved as it moves forward in time and that small perturbations decay leaving the system state unchanged.

Ideally, mathematical descriptions of behavior should match the physical phenomena observed. Many mathematical models involve justifiable reductions that simplify the models but preserve key physical characteristics of the system. However, these simplifications may result in the behavior of the mathematical model and the physical phenomena diverging as parameters vary. Parameters associated with change in stability properties of the mathematical model provide likely candidates for points of divergence from the physical phenomena. Hence, traveling wave stability analysis plays an important role in model verification.

To demonstrate the stability of traveling wave solutions, it suffices to show that there are no eigenvalues of the linearized operator in the deleted right half complex plane due to Zumbrun and his collaborators [46, 21, 35, 36] who generalized earlier work of [37, 18, 33, 34, 43]. Bounds on the unstable spectra can often be found using energy estimates, but usually a region in parameter space must still be checked for unstable eigenvalues. An effective way of checking for eigenvalues in a bounded region employs the Evans function, an analytic function whose zeros correspond in location and multiplicity to the eigenvalues of the linearized operator. The Evans function is determined by writing the eigenvalue problem as a first order system and then evolving the system toward zero where we initialize at $-\infty$ with the unstable manifold and at $+\infty$ with the stable manifold. The evolved solutions are then evaluated at zero and the Wronskian taken to determine linear independence. Hence zeros of the Evans function correspond to the intersection of the unstable manifold at $-\infty$ and the stable manifold at $+\infty$ thus forming an eigenfunction. Care

must be taken to initialize the system in a way that preserves analyticity of the Evans function. This allows us to compute the Evans function on a contour enclosing a bounded region where eigenvalues may occur and then apply the argument principle to determine if there are roots inside the contour. If the winding number is zero, then the traveling wave is stable, and if the winding number is nonzero the wave is unstable.

Numerical implementation of the Evans function is difficult due to inherent stiffness in the problem associated with resolving different growth and decay modes. Traditionally, this problem was solved in an elegant fashion by lifting the problem into an exterior product space so that the unstable and stable manifolds corresponded to a single stable mode in the new system. However, the size of the lifted problem grows as $\binom{n}{k}$ where n is the dimension of the system and k is the dimension of the stable or unstable subspace being evolved. Clearly this method becomes numerically unwieldy very quickly as the system size increases. We review the recent development of an orthogonalization method [28] that keeps the original dimension of the system and also maintains analyticity of the Evans function. In addition we discuss STABLAB, an interactive MATLAB based toolbox developed with convenience and flexibility in mind. As part of STABLAB, we consider root solving for the Evans function, a significant problem since function evaluations are costly making traditional root solving techniques, like Newton's method, undesirable.

We use STABLAB to verify Evans function output for traveling waves in Burgers equation, the generalized Korteweg-de Vries equation (gKdV) [39, 38], and the p-system with and without capillarity [3, 24, 23]. We then conduct a new study in isentropic magnetohydrodynamics (MHD) [4] obtaining results consistent with stability.

Chapter 2. Mathematical Background

In this chapter we discuss some of the mathematical issues pertaining to traveling wave stability; see [22] for details. Zumbrun and collaborators have shown for a large class of equations that spectral stability of the linearized operator implies nonlinear stability; see [46, 21, 35, 36]. Spectral stability can be determined using the Evans function, an analytic function whose zeros correspond in location and multiplicity to eigenvalues of the linearized system.

2.1 Traveling Waves

Consider the evolution equation,

$$u_t + f(u)_x - (B(u)u_x)_x + (C(u)u_{xx})_x = 0, \tag{2.1}$$

where $x \in \mathbb{R}$, and u, $f \in \mathbb{R}^n$, and B, C, $Q \in \mathbb{R}^{n \times n}$ are sufficiently smooth.

Definition 2.1. A traveling wave profile of (2.1) is a solution of the form

$$u(x, t) = \hat{u}(x - st), \tag{2.2}$$

where s is wave speed.

Equivalently we make the transformation $(x, t) \to (x - st, t)$ and seek stationary solutions of

$$u_t = \mathcal{F}(u) = (s - f'(u))u_x + (B(u)u_x)_x - (C(u)u_{xx})_x. \tag{2.3}$$

In this last method we transform our coordinates to a moving frame of reference so that the traveling wave appears stationary. Then the existence of a traveling wave solution reduces to that of an ODE,

$$(f'(u) - s)u' - (B(u)u')' + (C(u)u'')' = 0, \tag{2.4}$$

with appropriate boundary conditions. We restrict our attention to continuous traveling waves

3

with asymptotically constant end states,

$$\lim_{x \to \pm\infty} \hat{u}(x) = u_\pm \quad \text{and} \quad \lim_{x \to \pm\infty} \hat{u}^{(n)}(x) = 0, \quad n \geq 1. \tag{2.5}$$

A traveling wave solution is called a shock layer when $u_+ \neq u_-$ and a pulse when $u_+ = u_-$.

Remark. Considered as a dynamical system, the end states $u_\pm$ are equilibrium points of (2.4) so that connecting equilibria in the phase plane correspond to traveling waves. Note that (2.4) is translationally invariant since it is autonomous in x so that $\{\hat{u}(x + \delta)\}_{\delta \in \mathbb{R}}$ forms a smooth one parameter manifold of profiles for a single connecting orbit.

We finish this section with a few examples of traveling waves.

Example 2.2. (Viscous Burgers equation) We consider the one-dimensional Burgers equations,

$$u_t + uu_x = \nu u_{xx}, \tag{2.6}$$

where the constant $\nu > 0$ represents viscosity. Substituting $\hat{u}(x - st) = u(x,t)$ in (2.6) yields the profile equation

$$-s\hat{u}' + \hat{u}\hat{u}' = \nu\hat{u}'', \tag{2.7}$$

subject to $\hat{u}(\pm\infty) = u_\pm$. Integrating from $-\infty$ to x gives

$$-s(\hat{u} - u_-) + \frac{1}{2}(\hat{u}^2 - u_-^2) = \nu\hat{u}'. \tag{2.8}$$

Taking $x \to +\infty$ we find

$$-s(u_+ - u_-) + \frac{1}{2}(u_+^2 - u_-^2) = 0, \tag{2.9}$$

so that the Rankine-Hugoniot condition is

$$s = \frac{u_+ + u_-}{2}. \tag{2.10}$$

Returning to (2.7) and solving for $\hat{u}'$ we have

$$\hat{u}' = \frac{1}{2\nu}(\hat{u} - u_-)(\hat{u} - u_+), \tag{2.11}$$

4

which has solution

$$\hat{u}(x) = s - a \tanh\left(\frac{a(x - st + \delta)}{2\nu}\right),$$ (2.12)

where $a = (u_- - u_+)/2$ and $\delta \in \mathbb{R}$ is some translate.
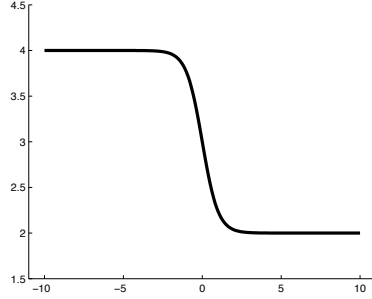
Figure 2.1: Profile for Burgers equation

Example 2.3. (gKdV) We consider the system

$$u_t + u_{xxx} + (u^p/p)_x = 0,$$ (2.13)

where $p \geq 2$, $p \in \mathbb{N}$. We translate $(x, t) \to (x - st, t)$ and seek stationary solutions of

$$u_t - su_x + u_{xxx} + (u^p/p)_x = 0.$$ (2.14)

The additional rescaling $(u, x, t) \to (s^{1/(1-p)}u, s^{1/2}x, s^{3/2}t)$ removes s;

$$u_t - u_x + u_{xxx} + (u^p/p)_x = 0.$$ (2.15)

Hence, the profile equation is

$$u''' - u' + (u^p/p)' = 0, \quad u^{(n)}(\pm\infty) = 0, \quad n = 0, 1, 2.$$ (2.16)

Integrating twice and using separation of variables results in the solution,

$$\hat{u}(x) = \left(\frac{p(p+1)}{2} \right)^{1/(p-1)} \operatorname{sech}((1-p)x/2 + \delta)^{2/(p-1)}, \tag{2.17}$$

where $\delta \in \mathbb{R}$ is some translate; see Figure 2.2.
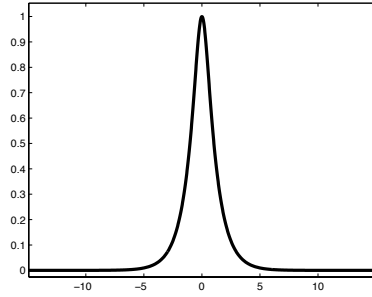
Figure 2.2: Profile for gKdV with $p = 5$

2.2 STABILITY OF TRAVELING WAVES

After determining the existence of a traveling wave, we are interested in knowing whether it is stable. If the solution $\hat{u}$ is "bumped" a little, that is perturbed, will the system return to the shock layer (possibly translated) or behave in some other fashion, e.g. bifurcate into something else?

Definition 2.4. We say $\hat{u}(x)$ is (asymptotically) orbitally stable with respect to some set of admissible perturbations $\mathcal{A}$ if $u(x,t) = \hat{u}(x) + v(x,t) \to \hat{u}(x + \delta)$ whenever $v \in \mathcal{A}$ and where $\delta \in \mathbb{R}$ is some translate.

2.3 SPECTRAL STABILITY

Determining asymptotic orbital stability reduces to a study of the spectrum of the traveling wave profile; see [46, 21, 35, 36]. The eigenvalue problem comes from the linearization of (2.3) about the stationary solution $\hat{u}(x)$ and the formation of the eigenvalue problem,

$$\lambda v = Lv := -(A(\hat{u})v)_x + (B(\hat{u})v_x)_x - (C(\hat{u})v_{xx})_x, \tag{2.18}$$

6

where $A(\hat{u})v = df(\hat{u})v - dB(\hat{u})v\hat{u}_x - dC(\hat{u})v\hat{u}_{xx}$.

Definition 2.5. We have:

(i). The spectrum $\sigma(L)$ of L is the set of all $\lambda \in \mathbb{C}$ such that $L - \lambda I$ is not invertible.

(ii). The point spectrum $\sigma_p(L)$ of L is the set of all isolated eigenvalues of L with finite multiplicity.

(iii) The essential spectrum $\sigma_e(L)$ of L is the entire spectrum less the point spectrum, that is $\sigma_e(L) = \sigma(L) \setminus \sigma_p(L)$.

Definition 2.6. We say that L in (2.18) is spectrally stable if there is no spectrum in the closed deleted right half plane, $\Sigma_+ = \{\lambda \in \mathbb{C}\setminus\{0\} | \Re e\lambda \geq 0\}$; see Figure 2.3.
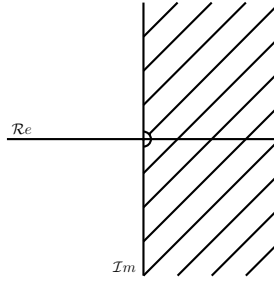
Figure 2.3: Deleted right half plane

Zumbrun and his collaborators [46, 21, 35, 36] have shown, generalizing the earlier work of [37, 18, 33, 34, 43], that spectral stability implies asymptotic orbital stability; see [23, 3, 4] for examples of application. In the case of instability, bifurcation diagrams may be constructed to observe its onset.

We note that the operator L always has nontrivial point spectrum since zero is an eigenvalue of L associated with translational invariance of (2.4).

Lemma 2.7. *(Sattinger [41]) The derivative of the profile $\hat{u}'$ is an eigenfunction of L with eigenvalue 0.*

Proof. By translational invariance, we have for (2.3) that $\mathcal{F}(\hat{u}(x + \delta)) = 0$ for all $\delta \in \mathbb{R}$. Then differentiating with respect to δ and setting $\delta = 0$, we have

$$0 = \frac{\partial}{\partial \delta}\mathcal{F}(\hat{u}(x + \delta))|_{\delta=0} = \mathcal{F}'(\hat{u}(x))\hat{u}'(x) = L(\hat{u}'(x)). \tag{2.19}$$

7

□

To be spectrally stable, both the essential and point spectrum of L must be excluded from Σ_+.

2.3.1 Essential Spectrum.

Excluding the essential spectrum is simplified by the following theorem:

Theorem 2.8 (Henry [20])**.** *The essential spectrum of L in (2.18) is sharply bounded to the right of*

$$\sigma_e(L_+) \cup \sigma_e(L_-), \tag{2.20}$$

where $L_\pm$ correspond to the operators obtained by linearizing about the constant solutions $\hat{u} = u_\pm$, respectively.

We linearize (2.3) about the constant solutions $u_\pm$ to get the linear PDE

$$\lambda v = Lv := -A_\pm v_x + B_\pm v_{xx} - C_\pm v_{xxx}, \tag{2.21}$$

where $A_\pm := df(u_\pm)$, $B_\pm := B(u_\pm)$, $C_\pm := C(u_\pm)$.

Since constant coefficient linear operators have no point spectrum, we note $\sigma(L_\pm) = \sigma_e(L_\pm)$. We determine $\sigma_e(L_\pm)$ using the Fourier transfrom.

Note that

$$(\widehat{L - \lambda I})^{-1}v = (-i\xi A_\pm - \xi^2 B_\pm + i\xi^3 C_\pm - \lambda I)^{-1}v, \quad \xi \in \mathbb{R}. \tag{2.22}$$

We see $L - \lambda I$ is not invertible when $-i\xi A_\pm - \xi^2 B_\pm + i\xi^3 C_\pm - \lambda I$ is singular. Thus

$$\lambda \in \sigma(L_\pm) \quad \text{iff} \quad \lambda \in \sigma(-i\xi A_\pm - \xi^2 B_\pm + i\xi^3 C_\pm), \tag{2.23}$$

for some $\xi \in \mathbb{R}$. This defines $2n$-curves $\lambda_j^\pm(\xi)$ corresponding to the eigenvalues of the right-hand side. Hence

$$\sigma_e(L_+) \cup \sigma_e(L_-) = \bigcup_j \lambda_j^+(\xi) \cup \bigcup_j \lambda_j^-(\xi). \tag{2.24}$$

In summary, sharp bounds on the essential spectrum of L are determined by the structure of $A_\pm, B_\pm, C_\pm$. This allows us to explicitly compute $\sigma_e(L)$ and see if it intersects Σ_+; see A.4 for an

8

example of computing the essential spectrum for Burgers equation.

2.3.2   Point Spectrum.   Energy estimates provide a historically successful method for finding bounds on the point spectrum of the linearized operator by leveraging the structure of the system. However, finding uniform bounds excluding the imaginary axis while allowing zero is difficult if not impossible. This difficulty can be remedied by transforming (2.18) to integrated coordinates. We set

$$\tilde{v}(x) = \int_{-\infty}^{x} v(z)dz, \tag{2.25}$$

substitute into (2.18), and integrate to obtain,

$$\lambda \tilde{v} = \mathcal{L}\tilde{v} := -A(\hat{u})\hat{v}' + B(\hat{u})\tilde{v}'' - C(\hat{u})\tilde{v}'''. \tag{2.26}$$

Lemma 2.9. *The operator L in (2.18) and $\mathcal{L}$ in (2.26) have the same point spectrum with the exception of $\lambda = 0$.*

Proof. Suppose that $\lambda \neq 0$ and $Lv = \lambda v$. We substitute $\tilde{v}'$ for v into (2.18) and integrate to obtain (2.26). We note that $\tilde{v}$ and its derivatives decay to zero at $\pm\infty$,

$$\lambda \tilde{v}(+\infty) = \lambda \int_{-\infty}^{\infty} v = \int_{-\infty}^{\infty} -(A(\hat{u})v)_x + (B(\hat{u})v_x)_x - (C(\hat{u})v_{xx})_x = 0,$$

yielding the needed boundary conditions so $\sigma_p(L)\backslash\{0\} \subset \sigma_p(\mathcal{L})$. Now suppose $\mathcal{L}\tilde{v} = \lambda \tilde{v}$ with $\tilde{v}^{(n)}(\pm\infty) = 0$, $n \geq 0$. We set $v = \tilde{v}'$ so that $\tilde{v}(x) = \int_{-\infty}^{x} v(z)dz$ and substitute $v = \tilde{v}'$ into (2.26) to obtain

$$\lambda \int_{-\infty}^{x} v(z)dz = -A(\hat{u})v + B(\hat{u})v' - C(\hat{u})v''. \tag{2.27}$$

Differentiating (2.27) yields (2.18) and thus $\sigma_p(\mathcal{L}) \subset \sigma_p(L)$.   □

Remark. We note that when $u_- \neq u_+$ that $w(x) = \int_{-\infty}^{x} \hat{u}'(z)dz = \hat{u}(x) - \hat{u}(-\infty)$ is not an eigenvector of $\mathcal{L}$ associated with $\lambda = 0$ since $w(+\infty) \neq 0$.

We give examples of energy estimates in sections 5.2 and A.3 and examples of using integrated coordinates in our model systems in chapters 4 and 5 and in section A.6.

2.4   Evans function

Energy estimates often give only a bound on where unstable spectra may exist. The Evans function is an analytic function that can be used to study stability in a bounded region using the argument principle. Furthermore, the Evans function gives structural information about the system; see [24]. We write the eigenvalue problem (2.18) or (2.26), $(L - \lambda)v = 0$, as a first order system,

$$W' = A(x, \lambda)W. \tag{2.28}$$

We note that $\lim_{x \to \pm \infty} A(x, \lambda) = A_{\pm}(\lambda)$, where A is analytic in λ. We assume that the dimension k of the unstable subspace U_- of A_- and the stable subspace S_+ of A_+ sum to n, the dimension of the entire phase space. We then initialize (2.28) at $-\infty$ with k vectors spanning U_- and with $n - k$ vectors spanning S_+ at $+\infty$ and solve both toward $x = 0$. This yields analytic basis $W_1^-, W_2^-, ..., W_k^-$ and $W_{k+1}^+, W_{k+2}^+, ..., W_n^+$ spanning the manifolds $W^{\mp}$ of solutions of (2.28) that decay as $x \to -\infty$ and $x \to +\infty$ respectively. We then define the Evans function as

$$D(\lambda) := \det(W_1^- \cdots W_k^- W_{k+1}^+ \cdots W_n^+)_{|x=0}. \tag{2.29}$$

Hence, a zero of the Evans function corresponds to the manifolds W^- and W^+ intersecting signifying an eigenfunction exists.

Remark. The eigenvalues of the linear operator L correspond in both multiplicity and location to the zeros of $D(\lambda)$ analogous to the characteristic polynomial of a finite dimensional operator.

Although we can solve analytically the Evans function for a few relatively simple systems, for example Burger's (see A.5 and A.6), most systems are too complicated to solve the Evans function analytically and hence require numerical computation.

If $\dim(k) > \dim(n/2)$ it is often advantageous to use the adjoint formulation of the Evans function; see [6]. Instead of finding the k dimensional unstable space of $W' = A(x, \lambda)W$ at $-\infty$,

we find the $n - k$ dimensional unstable subspace of $\tilde{W}' = -A(x, \lambda)^* \tilde{W}$ at $x = -\infty$. Then since

$$
\begin{aligned}
(\tilde{W}_i^*(x) W_j(x))' &= \tilde{W}_i^*(x) W_j'(x) + (\tilde{W}_i^*)'(x) W_j(x) \\
&= \tilde{W}_i^*(x) A(x, \lambda) W_j - (A(x, \lambda)^* \tilde{W}_i(x))^* W_j(x) \\
&= \tilde{W}_i^*(x) A(x, \lambda) W_j - \tilde{W}_i^*(x) A(x, \lambda) W_j(x) \\
&= 0,
\end{aligned}
\tag{2.30}
$$

we have that $\tilde{W}_i^*(x) W_j(x) \equiv$ constant. We note that $\tilde{W}_i^*(-\infty) W_j(-\infty) = 0$ since $\tilde{W}_i^*$ is a left eigenvector of $A(-\infty, \lambda)$ corresponding to a different eigenvalue than that of the right eigenvector $W_j(-\infty)$. Thus $\tilde{W}_i$ and W_j are orthogonal so that the original manifolds W_- and W_+ intersect when $\tilde{W}_-$ is orthogonal to W_+. We then define the Evan function to be

$$
D(\lambda) := \det(\tilde{W}_-^* \cdot W_+).
$$

We may similarly define the Evans function using the adjoint at $+\infty$.

CHAPTER 3. NUMERICAL EVANS FUNCTION COMPUTATION

In this chapter we discuss numerical implementation of the theory introduced in Chapter 2. We begin by showing how to numerically compute profiles. We then discuss various methods for overcoming the challenge of solving stiff ordinary differential equations associated with the Evans function. Finally we discuss root finding for the Evans function and computational issues.

3.1 BOUNDARY VALUE PROBLEM

Consider the wave profile ODE

$$y' = f(y), \tag{3.1}$$

with stationary points $u_\pm$, $f(u_\pm) = 0$, and where $y = (y_1, y_2, ..., y_n) \in \mathbb{R}^n$. Our boundary value problem (BVP) consists of (3.1) together with appropriate boundary conditions, suppose

$$\Pi_s^- y(-\infty) = 0, \quad \Pi_u^+ y(+\infty) = 0,$$

and a single phase condition, $l \cdot y(0) = \alpha$. Here Π_s^- projects onto the stable subspace of $df(u_-)$ and Π_u^+ projects onto the unstable subspace of $df(u_+)$. Our projective boundary conditions force the BVP solver to approach the desired end states orthogonal to the undesired manifold. Because of translational invariance, (3.1) together with projective conditions does not have a unique solution. Hence, we break the domain in half and solve

$$
\begin{aligned}
y'(x) &= f(y(x)) \\
z'(x) &= -f(z(x))
\end{aligned}
\tag{3.2}
$$

on $[0, \infty)$ subject to $y(0) = z(0)$ and $y_1(0) = \text{constant}$, and projective boundary conditions. We give an example of solving a boundary value problem using these methods in A.2 and in the examples below.

We note that solving the profile equation may be quite challenging. Sometimes dummy variables

must be introduced to obtain the correct dimensionality or to solve for wave speed. As parameters vary, solutions often become difficult to obtain and so continuation, stepping through parameter space with previous solutions as the initial guess in the boundary value solver, must be used. Even correctly employing boundary conditions can be tricky.

Example 3.1. The p-system with real viscosity is given in Lagrangian coordinates by

$$v_t - u_x = 0$$
$$u_t + p(v)_x = \left(\frac{u_x}{v}\right)_x$$

(3.3)

where v is the specific volume, u is the velocity, and $p(v)$ is the pressure law which we assume to be adiabatic satisfying $p(v) = a_0 v^{-\gamma}$, $a_0 > 0$ and $\gamma \geq 1$. The profile equation for a rescaled version of the p-system, which we derive in 4.3, is given by

$$v' = v(v - 1 + a(v^{-\gamma} - 1)),$$

(3.4)

where $a = v_+^\gamma \frac{1-v_+}{1-v_+^\gamma}$ subject to boundary conditions $v_- = 1$, $0 < v(+\infty) = v_+ < 1$ and $v'(\pm\infty) = 0$; see [3] for details. As described above, we break the domain in half doubling the size of the system,

$$v' = v(v - 1 + a(v^{-\gamma} - 1)),$$
$$z' = -z(z - 1 + a(z^{-\gamma} - 1)).$$

(3.5)

One boundary condition, $v(0) = z(0)$, connects the two solutions associated with the negative and positive domains. The other boundary condition, $v(0) = (v_- + v_+)/2$, fixes a point on the manifold of solutions associated with translational invariance. We use MATLAB's **bvp4c** solver, which uses collocation, to solve the boundary value problem using the tanh function in the initial guess. This yields the profile given in Figure 3.1.

Example 3.2. The p-system with capillarity in Lagrangian coordinates is given by,

$$v_t - u_x = 0,$$
$$u_t + p(v)_x = \left(\frac{u_x}{v}\right)_x - dv_{xxx},$$

(3.6)

13
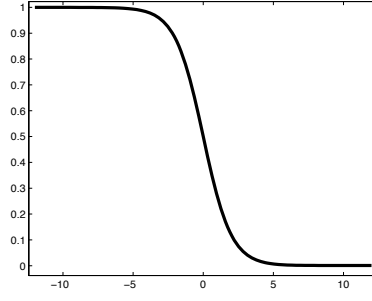
Figure 3.1: Profile for the p-system

where v represents specific volume, u is velocity, $p(v)$ is the pressure law for an ideal gas, and $d \geq 0$ represents capillarity strength. We consider an adiabatic gas law, $p(v) = v^{-\gamma}$.

After some preliminary rescalings and integration, the profile equation, derived in 4.4, is given by,

$$v - v_- + a(v^{-\gamma} - v_-^{-\gamma}) = \frac{v'}{v} - dv'' \tag{3.7}$$

where

$$a = -\frac{v_+ - v_-}{v_+^{-\gamma} - v_-^{-\gamma}}, \tag{3.8}$$

and $v_- = 1$ and $0 < v_+ < 1$; see [23] for details. We write 3.7 as a first order system setting $y_1 = v$ and $y_2 = v'$,

$$
\begin{aligned}
y_1 &= y_2, \\
y_2 &= \frac{-1}{d}(y_1 - 1 + a(y_1^{-\gamma} - 1)) - \frac{y_2}{y_1}.
\end{aligned}
\tag{3.9}
$$

Splitting the domain in half and doubling the dimension of the system, we have

$$
\begin{aligned}
y_1 &= y_2, \\
y_2 &= \frac{-1}{d}(y_1 - 1 + a(y_1^{-\gamma} - 1)) - \frac{y_2}{y_1}, \\
y_3 &= -y_4, \\
y_4 &= \frac{1}{d}(y_3 - 1 + a(y_3^{-\gamma} - 1)) + \frac{y_4}{y_3},
\end{aligned}
\tag{3.10}
$$

14

where at $x = +\infty$ we have $y_1 = v_+$, $y_2 = 0$, $y_3 = v_-$, and $y_4 = 0$. We take for boundary conditions in our solver the two matching conditions $y_1(0) = y_3(0)$ and $y_2(0) = y_4(0)$, the phase condition $y_1(0) = (1+v_+)/2$ fixing a unique solution on the manifold of solutions associated with translational invariance, and we take $L \cdot ([y_1\ y_2\ y_3\ y_4]^T - [v_+\ v'_+\ v_-\ v'_-]^T) = L \cdot ([y_1\ y_2\ y_3\ y_4]^T - [v_+\ 0\ 1\ 0]^T) = 0$ where L is a basis for the unstable space at $x = +\infty$ causing the boundary solver to approach the ends states orthogonal to the growth manifold. We modify the tanh function to obtain our initial guess and solve using **bvp5c**, one of MATLAB's collocation boundary value solvers, to obtain the profiles in Figure 3.2.
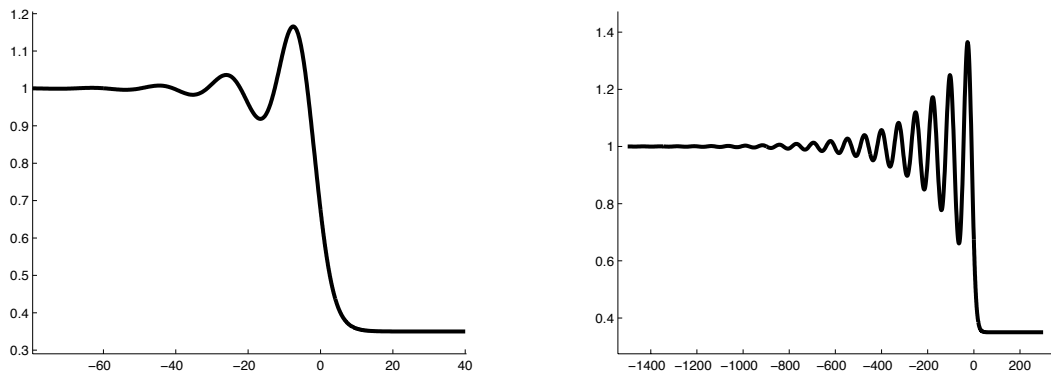
Figure 3.2: The profile equation for the p-system with capillarity. As capillarity strength increases, the profile becomes highly oscillatory.

3.2   THE COMPOUND MATRIX METHOD

In this section we consider numerical implementation of the Evans function discussed in section 2.4. We see how stiff ODE problems arise and how the compound matrix method overcomes this difficulty; see [9] for details.

Consider the linear system

$$W' = A(x, \lambda)W \tag{3.11}$$

with boundary conditions $W(\pm\infty) = 0$, $W \in \mathbb{C}^n$, $\lambda \in \mathbb{C}$ (fixed), $' = \frac{d}{dx}$. We seek non-trivial solutions to the BVP. Let $\{r_j\}_{j=1}^k$ and $\{r_j\}_{j=k+1}^n$ be the generalized right eigenvectors of

$A^-(\lambda) = \lim_{x \to -\infty} A(x, \lambda)$ and $A^+(\lambda) = \lim_{x \to \infty} A(x, \lambda)$ respectively, with corresponding eigenvalues $\{\mu_j^-\}_{j=1}^k$ and $\{\mu_j^+\}_{j=k+1}^n$ where $\mathcal{R}e(\mu_j^-) > 0$ and $\mathcal{R}e(\mu_j^+) < 0$. That is, $\{u_j^-\}_{j=1}^k$ are the growth modes at $x = -\infty$ and $\{\mu_j^+\}_{j=k+1}^n$ are the decay modes at $x = \infty$. Then the unstable manifold $U^-(x)$ of $x = -\infty$ is given by $U^-(x) = W_1^-(x) \wedge ... \wedge W_k^-(x)$ where W_j satisfies

$$\begin{cases} W_j^{-\,\prime} = A(x, \lambda) W_j^- \\ W_j^-(x) \sim e^{\mu_j^- x} r_j^- \qquad\qquad x \ll 0, \qquad j = 1, ..., k \end{cases} \tag{3.12}$$

and the stable manifold $S^+(x)$ of $x = +\infty$ is given by $S^+(x) = W_{k+1}^+(x) \wedge ... \wedge W_n^+(x)$ where W_j^+ satisfies

$$\begin{cases} W_j^{+\,\prime} = A(x, \lambda) W_j^+ \\ W_j^+(x) \sim e^{\mu_j^+ x} r_j^+ \qquad\qquad x \gg 0, \qquad j = k+1, ..., n. \end{cases} \tag{3.13}$$

Then a non-trivial solution exists when the unstable and stable manifolds intersect, that is when the quantity

$$U^-(x) \wedge S^+(x) \cong \det[W_1^- W_2^- ... W_k^- W_{k+1}^+ ... W_n^+] = 0;$$

see appendix B for a discussion of exterior products. If the eigenvectors $\{r_j^-\}_{j=1}^k$ and $\{r_j^+\}_{j=k+1}^n$ vary analytically in λ, then we define the Evans function to be

$$\begin{aligned} D(\lambda) &= U^-(x, \lambda) \wedge S^+(x, \lambda)|_{x=0} \\ &\cong \det[W_1^- W_2^- ... W_k^- W_{k+1}^+ ... W_n^+]|_{x=0}. \end{aligned} \tag{3.14}$$

Numerically, the Evans function is difficult to compute. As an example, suppose $n = 4$, $k = 2$. We have eigenpairs (μ_1^-, r_1^-), (μ_2^-, r_2^-), (μ_3^+, r_3^+), (μ_4^+, r_4^+). Assume $\mathcal{R}e(\mu_1^-) > \mathcal{R}e(\mu_2^-) > 0$ and $\mathcal{R}e(\mu_3^+) < \mathcal{R}e(\mu_4^+) < 0$. The numerical problem is that it is hard to resolve multi-mode growth and decay because any round-off error (or numerical error) favors the largest growth/decay mode; see Figure 3.3. Hence in the long run, $W_2^-(x)$ becomes $aW_1^-(x) + bW_2^-(x)$.

This causes either bad data, or slow computation. The compound-matrix method overcomes this difficulty. We lift the problem from $\mathbb{C}^n$ to $\wedge^k(\mathbb{C}^n)$ (wedge product space). Note that $\wedge^k(\mathbb{C}^n) \cong \mathbb{C}^{\binom{n}{k}}$.
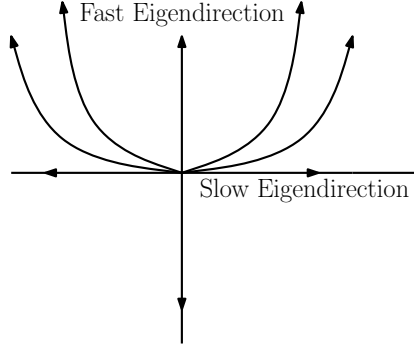
Figure 3.3: Numerical instability due to growth in the fast eigendirection

Example. Consider the $n = 4$, $k = 2$ case. Let $\{e_1, ..., e_4\}$ be the standard basis for $\mathbb{C}^4$. Then $\wedge^2(\mathbb{C}^4)$ has the basis $(e_1 \wedge e_2, e_1 \wedge e_3, e_1 \wedge e_4, e_2 \wedge e_4, e_3 \wedge e_4)$. Then we lift $A(x, \lambda)$ into $\wedge^2(\mathbb{C}^4)$ by defining $A^{(2)} \circ e_i \wedge e_j = (Ae_i) \wedge e_j + e_i \wedge (Ae_j)$. Thus if

$$
A = \begin{pmatrix} a_{11} & a_{12} & a_{13} & a_{14} \\ a_{21} & a_{22} & a_{23} & a_{24} \\ a_{31} & a_{32} & a_{33} & a_{34} \\ a_{41} & a_{42} & a_{43} & a_{44} \end{pmatrix},
\tag{3.15}
$$

then

$$
A^{(2)} = \begin{pmatrix}
a_{11} + a_{22} & a_{23} & a_{24} & -a_{13} & -a_{14} & 0 \\
a_{32} & a_{11} + a_{33} & a_{34} & a_{12} & 0 & -a_{14} \\
a_{42} & a_{43} & a_{11} + a_{44} & 0 & a_{12} & a_{13} \\
-a_{31} & a_{21} & 0 & a_{22} + a_{33} & a_{34} & -a_{24} \\
-a_{41} & 0 & a_{21} & a_{43} & a_{22} + a_{44} & a_{23} \\
0 & -a_{41} & a_{31} & -a_{42} & a_{32} & a_{33} + a_{44}
\end{pmatrix}.
\tag{3.16}
$$

The numerical advantage in our new system $A^{(2)}$ is that a single trajectory corresponds to our manifold of A.

Lemma 3.3. *If $\{\mu_i, r_i\}_{i=1}^n$ are eigenpairs for A, then $\sum_{i=1}^k \mu_{\sigma(i)}$ is an eigenvalue of $A^{(k)}$, where $\sigma \in S^n$, with corresponding eigenvector $r_{\sigma(1)} \wedge r_{\sigma(2)} \wedge ... \wedge r_{\sigma(k)}$.*

17

Proof.

$$A^{(k)} \circ r_{\sigma(1)} \wedge r_{\sigma(2)} \wedge ... \wedge r_{\sigma(k)} = Ar_{\sigma(1)} \wedge r_{\sigma(2)} \wedge ... \wedge r_{\sigma(k)}$$
$$+ r_{\sigma(1)} \wedge Ar_{\sigma(2)} \wedge ... \wedge r_{\sigma(k)}$$
$$+ r_{\sigma(1)} \wedge r_{\sigma(2)} \wedge ... \wedge Ar_{\sigma(k)}$$
$$= [\mu_{\sigma(1)} + ... + \mu_{\sigma(k)}]r_{\sigma(1)} \wedge r_{\sigma(2)} \wedge ... \wedge r_{\sigma(k)}.$$

(3.17)

$\square$

Corollary 3.4. *If $\{\mu_i\}_{i=1}^k$ are the largest eigenvalues of A, then $\sum_{i=1}^k \mu_i$ is the largest eigenvalue of $A^{(k)}$.*

Proof. All eigenvalues of $A^{(k)}$ are of the form $\sum_{i=1}^k \mu_{\sigma(i)}$. Thus the k largest of A form the largest eigenvalue of $A^{(k)}$. $\square$

It has been demonstrated that the following numerical technique yields good stability. We begin with

$$W' = A^{(k)}(x, \lambda)W \qquad W \in \mathbb{C}^{n \text{ ch } k}$$
$$W(-L) = e^{\mu^- L}r^-.$$

(3.18)

Let $W = e^{\mu^- x}v(x)$. Then $W' = \mu^- e^{\mu^- x}v(x) + e^{\mu^- x}v'(x)$. Hence $\mu^- e^{\mu^- x}v(x) + e^{\mu^- x}v'(x) = A^{(k)}(x, \lambda)e^{\mu^- x}v(x)$. The new ODE becomes

$$\begin{cases} v'(x) = (A^{(k)}(x, \lambda) - \mu^-)v(x) \\ v(-L) = r^-. \end{cases}$$

(3.19)

3.3 THE POLAR COORDINATES METHOD

The compound matrix method provides an elegant way to overcome the inherent difficulty of solving a stiff system. However, the dimension of the lifted problem grows as $\binom{n}{k}$ which becomes large quickly, e.g. $\binom{10}{5} = 252$ and $\binom{20}{10} = 184,756$. Several orthogonalization methods have been developed to solve stiff Evans function problems maintaining the original dimension of the system. However, these methods lose the important property of analyticity that allows implementation of

18

the argument principle. A continuous orthogonalization method for Evans function computation was given in [28] and demonstrated successfully in [3, 24, 23, 4], to name a few. We describe this method of continuous orthogonalization, also known as the polar coordinate method, a.k.a. analytic orthogonalization.

Lemma 3.5. *If $\{q_1^-, q_2^-, ..., q_k^-\}$ is an orthonormal set spanning $\{w_1^-, w_2^-, ..., w_k^-\}$ then there exists a $k \times k$ matrix α^- such that*

$$W^- = [w_1^-, w_2^-, ..., w_k^-]^{n \times k} = [q_1^-, q_2^-, ..., q_k^-]\alpha^- = Q^-\alpha^-. \tag{3.20}$$

Moreover,

$$w_1^- \wedge w_2^- \wedge ... \wedge w_k^- = (\det \alpha^-)q_1^- \wedge q_2^- \wedge ... \wedge q_k^-. \tag{3.21}$$

Proof. Since $\{q_i^-\}$ spans $\{w_i^-\}$, $w_j^- = Q^- x$ for some coefficient vector x. Define the jth column of α^- to be x. Then $W^- = Q^-\alpha^-$.

Now $w_i^- = \sum_{p=1}^{k} \alpha_{p,i}^- q_p^-$ which for ease of notation we denote $\sum_{p_i=1}^{k} \alpha_{p_i} q_{p_i}$. Then

$$
\begin{aligned}
w_1^- \wedge w_2^- \wedge ... \wedge w_k^- &= \left(\sum_{p_1=1}^{k} \alpha_{p_1} q_{p_1} \right) \wedge \left(\sum_{p_2}^{k} \alpha_{p_2} q_{p_2} \right) \wedge ... \wedge \left(\sum_{p_k=1}^{k} \alpha_{p_k} q_{p_k} \right) \\
&= \sum_{p_1=1}^{k} \sum_{p_2=1}^{k} ... \sum_{p_k=1}^{k} (\alpha_{p_1} \alpha_{p_2}...\alpha_{p_k}) q_{p_1} \wedge q_{p_2} \wedge ... \wedge q_{p_k} \\
&= \sum_{(j_1,j_2,...,j_k) \in P} (\alpha_{j_1} \alpha_{j_2}...\alpha_{j_k}) q_{j_1} \wedge q_{j_2} \wedge ... \wedge q_{j_k},
\end{aligned} \tag{3.22}
$$

where P is the set of all permutations of $(1, 2, ..., k)$, e.g. $(j_1, j_2, ..., j_k) = (2, 3, ..., k, 1) \in P$. Let $|(j_1, j_2, ..., j_k)|$ denote the sign of the permutation, that is $|(j_1, j_2, ..., j_k)| = 1$ if $(j_1, j_2, ..., j_k)$ can be written as an even number of permutations, and $|(j_1, j_2, ..., j_k)| = -1$ otherwise. Then by the alternating property of wedge products we have,

$$
\sum_{(j_1,j_2,...,j_k) \in P} (\alpha_{j_1} \alpha_{j_2}...\alpha_{j_k}) q_{j_1} \wedge q_{j_2} \wedge ... \wedge q_{j_k} = \sum_{(j_1,j_2,...,j_k) \in P} |(j_1, j_2, ..., j_k)|(\alpha_{j_1} \alpha_{j_2}...\alpha_{j_k}) q_1 \wedge q_2 \wedge ... \wedge q_k
$$

$$
= \det(\alpha) q_1 \wedge q_2 \wedge ... \wedge q_k.
$$

19

$\square$

Note that $W^- \wedge W^+ = (\det \alpha^-)(\det \alpha^+)Q^- \wedge Q^+$. Then we define the Evans function,

$$D(\lambda) = \det(W^-|W^+) = (\det \alpha^-)(\det \alpha^+)\det(Q^-|Q^+). \qquad (3.23)$$

Consider continuous orthogonalization. Let $W^-(x) = Q^-(x)\alpha^-(x)$. Then suppressing the bar notation we have,

$$W'(x) = Q'(x)\alpha(x) + Q(x)\alpha'(x).$$

Hence,

$$Q'(x)\alpha(x) + Q(x)\alpha'(x) = A(x,\lambda)Q(x)\alpha(x)$$
$$\Rightarrow \quad Q'(x)\alpha(x) = A(x,\lambda)Q(x)\alpha(x) - Q(x)\alpha'(x) \qquad (3.24)$$
$$\Rightarrow \quad Q'(x) = A(x,\lambda)Q(x) - Q(x)B(x),$$

where $B(x) = \alpha'(x)\alpha^{-1}(x)$. Note that α is invertible since otherwise $\{w_i\}$ would be linearly dependent for some value of x signifying two unique solutions in phase space share a common point.

Hence we seek to solve,

$$\begin{cases} Q'(x) = A(x,\lambda)Q(x) - Q(x)B(x) \\ \alpha'(x) = B\alpha. \end{cases} \qquad (3.25)$$

Recall that $Q^H Q = I_{k \times k}$. Thus

$$(Q^H Q)' = (Q^H)'Q + Q^H Q' = I' = 0. \qquad (3.26)$$

substituting for Q', we have

$$
\begin{aligned}
0 &= (Q^H Q)' \\
&= (Q^H A^H - B^H Q^H)Q + Q^H(AQ - QB) \\
&= Q^H A^H Q - B^H Q^H Q + Q^H A Q - Q^H Q B \\
&= Q^H(A^H + A)Q - B^H - B.
\end{aligned}
\tag{3.27}
$$

Theorem 3.6. *If (3.25) has orthogonal initial data, $Q_0^H Q_0 = I_{k \times k}$, then (3.27) is a necessary and sufficient condition for orthogonality.*

Proof. We have shown that (3.27) is a necessary condition for orthogonality. Since $(Q^H Q)' = 0$, then $Q^H Q \equiv$ constant so that if $Q_0^H Q_0 = I_{k \times k}$, then $Q^H Q = I_{k \times k}$. $\qquad\square$

There are various continuous orthogonalization methods. For example, Drury's method makes the choice $B = Q^H A Q$ and Davey's method sets $B = (Q^H Q)^{-1} Q^H A Q$. Recently, Zumbrun showed that Drury's method is stable in the context of Evans function computation [44], and in [28], Drury out performed other methods, such as Davey's. Another stable method for continuous orthogonalization is given by Dieci, Russell, and Vleck; see [15].

3.4 Method of Kato

If we initialize the first order system, $W' = A(x, \lambda)W$ given in (2.28) with analytically varying initial conditions, then $D(\lambda)$ will be analytic allowing us to use the argument principle to determine the presence of unstable spectra. We obtain an analytically varying initializing basis using eigenprojections of $A(x, \lambda)$ and a standard result due to Kato.

Let $P_\pm$ be the eigenprojection of $A_\pm := \lim_{x \to \pm\infty} A(x, \lambda)$ onto its stable/unstable subspace respectively. Assume A is consistently split, that is, that the dimension of the stable subspace and the dimension of the unstable subspace of $A_\pm$ are constant and sum to n, the dimension of A, for all $\lambda \in \Omega$ where Ω is some region of interest. Then the projectors $P_\pm$ are analtyic by standard matrix perturbation theory [30].

Proposition 3.7. *(Kato) [30] Let $P(\lambda)$ be an analytically varying projection on a simply connected*

domain $\Omega \subset \mathbb{C}$. *Then, the linear analtic ODE*

$$r'_j = P' r_j; \quad r_j(\lambda_0) = r^0_j \tag{3.28}$$

defines a global analytically varying basis $\{r_j(\lambda)\}$ *of the associated invariant subspace Range* $P(\lambda)$
where " ' " *denotes* $d/d\lambda$. *In particular if* $R(\lambda) = [r_1(\lambda) \; r_2(\lambda) \; ...r_k(\lambda)]$ *satisfies* (3.28) *where the*
initial condition $R_0 = R(\lambda_0)$ *is full rank (its columns form a basis for the desired unstable/stable*
subspace) and where $P_0 R_0 = R_0$, *then*

(i) $\mathrm{rank}(R) \equiv \mathrm{rank}(R_0)$

(ii) $PR \equiv R$, *and*

(iii) $PR' \equiv 0$.

Proof. Note that (3.28) is a linear ODE with analytic coefficients, and thus has an analytic solution
in a neighborhood of λ_0. By the principle of analytic continuation, there is a global analytic solution
to (3.28) on any simple connected domain containing λ_0; see [30, 27, 45]. We also get property (i)
since (3.28) is a linear ODE; see [45, 27, 30]. Before proving properties (ii) and (iii) we note that
$PP'P = 0$ since $P' = (P^2)' = P'P + PP'$ whereupon left multiplication by P yields $PP'P = 0$.
Now note that

$$
\begin{aligned}
(PR - R)' &= P'R + PR' - R' \\
&= P'R + (P - I)R' \\
&= P'R + (P - I)P'R \\
&= PP'R,
\end{aligned}
\tag{3.29}
$$

so that $(PR - R)' = -PP'(PR - R)$. Initializing this last ODE with $P(\lambda_0)R_0 - R_0 = 0$ and
employing uniqueness of solutions of ODEs, we have $PR = R$. For (iii) note that $PR' = PP'R$
and apply $R = PR$ to get $PR' = PP'PR = 0$. $\qquad\square$

We note that together conditions (i) and (ii) give us that $R(\lambda)$ is a basis of the desired subspace
and condition (iii) suggests that this basis is in some sense optimal since its variation on the desired
manifold is minimal.

3.4.1 Application. Using a forward difference scheme to approximate 3.28, we have

$$\frac{R_{j+1} - R_j}{\lambda_{j+1} - \lambda_j} = \frac{P_{j+1} - P_j}{\lambda_{j+1} - \lambda_j} R_j \tag{3.30}$$

so that $R_{j+1} = R_j + P_{j+1}R_j - P_jR_j = P_{j+1}R_j$ since $P_jR_j = R_j$.

For a second-order scheme we use the approximations,

$$\frac{R_{j+1} - R_j}{\lambda_{j+1} - \lambda_j} \approx P'_{j+1/2}R_{j+1/2},$$

$$R_{j+1/2} \approx P_{j+1/2}R_j,$$

$$P_{j+1/2} \approx \frac{1}{2}(P_{j+1} + P_j),$$

$$P'_{j+1/2} = \frac{P_{j+1} - P_j}{\lambda_{j+1} - \lambda_j},$$

to get the scheme

$$
\begin{aligned}
R_{j+1} &= R_j + (\lambda_{j+1} - \lambda_j)P'_{j+1/2}R_{j+1/2} \\
&= R_j + (\lambda_{j+1} - \lambda_j)\frac{P_{j+1} - P_j}{\lambda_{j+1} - \lambda_j}R_{j+1/2} \\
&= R_j + (P_{j+1} - P_j)P_{j+1/2}R_j \\
&= R_j + \frac{1}{2}(P_{j+1} - P_j)(P_{j+1} + P_j)R_j.
\end{aligned}
\tag{3.31}
$$

To insure R_{j+1} is in the range of P_{j+1} we multiply the scheme by P_{j+1} to obtain

$$R_{j+1} = P_{j+1}R_j + \frac{1}{2}P_{j+1}(P_{j+1} - P_j)(P_{j+1} + P_j)R_j, \tag{3.32}$$

which simplifies to

$$R_{j+1} = P_{j+1}[I + (1/2)P_j(I - P_{j+1})]R_j. \tag{3.33}$$

For details see [45].

3.5 Winding number and root finding

In this section we discuss a new method, inspired by [12], for finding the roots of the Evans function in the case of instability. Computing the Evans function is costly making traditional root solving techniques, like Newton's method, undesirable since new Evans function calls are required at each iterative step. The method of moments only uses the information given by the already evaluated contour to evaluate roots.

3.5.1 Derivation of Moments. Let f be analytic inside and on a simple closed positively oriented contour Γ and let f be nonzero on Γ. Suppose $z_1, \cdots, z_n$ are the n distinct roots of f inside Γ with respective multiplicities $m_1, m_2, ..., m_n$ and $c \neq z_k \ \forall k$ is a constant. Then for $p = 0, 1, 2, ...$

$$M_p(c) = \frac{1}{2\pi i} \oint_\Gamma \frac{(z-c)^p f'(z)}{f(z)} dz = \sum_{k=1}^n m_k(z_k - c)^p \tag{3.34}$$

where m_k is the multiplicity of z_k. Note that $M_p(c)$ is the pth moment of f about c.

Proof. The proof follows from an easy extension of the argument principle [40]. Let z_k be a zero of f inside of Γ. Since f is analytic at z_k, we have

$$f(z) = h(z)(z - z_k)^{m_k} \tag{3.35}$$

where $h(z)$ is analytic at z_k and $h(z_k) \neq 0$. Then $f'(z) = h'(z)(z - z_k)^{m_k} + m_k h(z)(z - z_k)^{m_k-1}$ and

$$g(z) = \frac{(z-c)^p f'(z)}{f(z)} = \frac{(z-c)^p h'(z)}{h(z)} + \frac{(z-c)^p m_k}{z - z_k}. \tag{3.36}$$

Since $h(z)$ is analytic at z_k, the residue of $g(z)$ at z_k is $m_k(z_k - c)^p$. Then by Cauchy's Residue Theorem,

$$\oint_\Gamma \frac{(z-c)^p f'(z)}{f(z)} dz = 2\pi i \sum_{k=1}^n m_k(z_k - c)^p. \tag{3.37}$$

$\square$

Note that $M_0(0)$ gives the number of zeros of $f(z)$ inside of Γ, and that $M_1(0)/M_0(0)$ and $M_2(\mu)/M_0(0)$ respectively give their center of mass and variance.

3.5.2   Using the Moments to Find Roots.   Let K_m be the mth order elementary symmetric polynomial in the roots $\{z_k\}_{k=1}^n$ of f inside Γ. Then

$$p(z) = (z - z_1)(z - z_2) \cdots (z - z_n) \tag{3.38}$$

$$= z^n - K_1 z^{n-1} + K_2 z^{n-2} + \cdots + (-1)^n K_n.$$

We determine K_m using the moments described in the previous section. For example, consider the case when f has two roots inside of Γ,

$$
\begin{aligned}
M_0(0) &= 2 \\
M_1(0) &= z_1 + z_2 \\
M_2(0) &= z_1^2 + z_2^2.
\end{aligned}
\tag{3.39}
$$

Since

$$M_1(0)^2 = z_1^2 + 2z_1 z_2 + z_2^2$$

$$= M_2(0) + 2z_1 z_2$$

we find

$$
\begin{aligned}
K_1 &= M_1(0) \\
K_2 &= \frac{1}{2}\big(M_1(0)^2 - M_2(0)\big).
\end{aligned}
\tag{3.40}
$$

Now $(z - z_1)(z - z_2) = z^2 - K_1 z + K_2$, so z_1 and z_2 are given by $z_{1,2} = \frac{1}{2}(K_1 \pm \sqrt{K_1^2 - 4K_2})$.

We note that this method is limited since there is no general closed solution to polynomials of degree greater than four, and since small perturbations in polynomial coefficients can lead to significantly different roots.

3.5.3   Computing $M_0(0)$.   If f is analytic and nonzero on the contour C and $W = f(C)$ does not pass through the branch cut of the log function, then

$$\int_C \frac{f'(z)}{f(z)}dz = \log(f(z_1)) - \log(f(z_0)), \tag{3.41}$$

where z_0 is the beginning point of C and z_1 is the end point. Now $\log(z) = \text{Log}|z| + i\text{Arg}(z) + i2k\pi$ where Log is the natural logarithmic function of real variables and Arg is the principal argument of z. Then

$$\int_C \frac{f'(z)}{f(z)}dz$$

is just the change in the angle between $f(z_0)$ and $f(z_1)$ where the angle jumps by 2π when it crosses the branch cut of log.

3.5.4   A Quadrature Method for $M_p(0)$.   We use Simpson integration with Lagrange interpolation to approximate

$$\oint_\Gamma (z-c)^p \frac{f'(z)}{f(z)}dz$$

using a centered difference approximation for $f'(z)$.

Then,

$$\int_{z_i}^{z_{i+2}} g(z)dz = \int_{z_i}^{z_{i+2}} (z-c)^p \frac{f'(z)}{f(z)}dz$$

$$\approx \int_{z_i}^{z_{i+2}} \frac{(z-z_{i+1})(z-z_{i+2})}{(z_i-z_{i+1})(z_i-z_{i+2})}g(z_i)dz + \int_{z_i}^{z_{i+2}} \frac{(z-z_i)(z-z_{i+2})}{(z_{i+1}-z_i)(z_{i+1}-z_{i+2})}g(z_{i+1})dz$$

$$+ \int_{z_i}^{z_{i+2}} \frac{(z-z_i)(z-z_{i+1})}{(z_{i+2}-z_i)(z_{i+2}-z_{i+1})}g(z_{i+2})dz.$$

$$\tag{3.42}$$

Let

$$a = \frac{g(z_i)}{(z_i-z_{i+1})(z_i-z_{i+2})},$$

$$b = \frac{g(z_{i+1})}{(z_{i+1}-z_i)(z_{i+1}-z_{i+2})}, \tag{3.43}$$

$$c = \frac{g(z_{i+2})}{(z_{i+2}-z_i)(z_{i+2}-z_{i+1})}.$$

26

We have

$$\int_{z_i}^{z_{i+2}} g(z)dz \approx \int_{z_i}^{z_{i+2}} a(z - z_{i+1})(z - z_{i+2}) + b(z - z_i)(z - z_{i+2}) + c(z - z_i)(z - z_{i+1})dz$$

$$= \frac{z_{i+2}^3 - z_i^3}{3}(a + b + c) - \frac{z_{i+2}^2 - z_i^2}{2}\big(a(z_{i+1} + z_{i+2}) + b(z_i + z_{i+2}) + c(z_i + z_{i+1})\big)$$

$$+ (z_{i+2} - z_i)\big(az_{i+1}z_{i+2} + bz_i z_{i+2} + cz_i z_{i+1}\big).$$

$$(3.44)$$

3.5.5   Apllication.   The gKdV equation, discussed in more detail in section 4.2, is given by

$$u_t + u_{xxx} + (1/p)(u^p)_x = 0, \quad p \geq 2, \quad p \in \mathbb{N}. \tag{3.45}$$

This system is known to undergo transition from stability to instability when $p = 5$; see [39, 38] for details. In Table 3.1 we show how the root given by the method of moments convergences to that given by Müller's method for the gKdV system with $p = 6$. We use Simpson integration with quadratic Lagrange interpolation to evaluate the relevant integral.

Mesh Points	8	18	28	38	48	58	68	78
Abs Difference	1.11	3.08(-1)	1.74(-1)	9.30(-2)	5.98(-2)	5.43(-2)	3.78(-2)	2.31(-2)

Table 3.1: Absolute value of the difference between the root given by the method of moments and Müller's method for the gKdV sysem with $p = 6$.

3.6   MULTI-CORE PROCESSING

Numerical Evans function computations are costly since each function evaluation requires solving an ODE to find an analytic basis. However, finding a basis for a point on the contour requires no information about the other points, hence is embarrassingly parallel. We use Matlab's new parallel processing toolbox to compute the Evans function on eight cores resulting in a dramatic increase in computation on the parallelized part.

3.7   STABLAB

The Evans function has proven to be an excellent tool for studying shock wave stability in parameter regimes that evade analytical proof, but also as a way of verifying or giving direction to analytical results. Given a new system, we would like to be able to start computing the wave profile and the Evans function within an hour. We would also like the flexibility to provide analytic components to the computation when they are available. To accomplish this goal, we developed STABLAB, an interactive MATLAB-based stability package.

In STABLAB, we provide options for computing the Evans function using either the compound matrix method or the polar method. The adjoint formulation of the Evans function is also available as well as a subroutine for finding an analytic basis using the method of Kato. Functions aiding profile computation deal with the issue of translational invariance, and machinery is in place for winding number calculations and root solving. Parallel computing is also available. See appendix C for STABLAB documentation.

We use STABLAB to study the model systems given in chapter 4 and note that it is succesfully used in [3, 24, 23, 26, 14, 25].

Chapter 4. Example Systems

In this chapter we apply the theory and methods introduced in chapters 2 and 3 to several model systems; we verify shock layer stability for Burgers equation and the p-system with and without capillarity. We also verify instability in gKdV.

4.1 Burgers

Consider Burgers equation,

$$u_t + u u_x = \nu u_{xx} \tag{4.1}$$

where the constant $\nu > 0$ represents viscosity (by rescaling we may assume $\nu = 1$) and x and t represent space and time respectively; see [8] for details. Assume that

$$u(x,t) = \hat{u}(x - st) \tag{4.2}$$

where s is wave speed. This substitution reduces the problem to one variable with a moving frame of reference. The solution to this ODE is the wave profile and is stationary because our frame of reference moves along at the same speed as the wave.

We assume asymptotically constant boundary conditions $\hat{u}(\pm\infty) = u_\pm$ where $u_- > u_+$.

Transferring $\hat{u}$ into (4.1) we obtain

$$-s\hat{u}' + \hat{u}\hat{u}' = \nu\hat{u}''. \tag{4.3}$$

Integrating yields

$$-s \int_{-\infty}^{x} \hat{u}' + \int_{-\infty}^{x} \hat{u}\hat{u}' = \nu \int_{-\infty}^{x} \hat{u}'', \tag{4.4}$$

which becomes

$$-s(\hat{u} - u_-) + \frac{1}{2}(\hat{u}^2 - u_-^2) = \nu\hat{u}'. \tag{4.5}$$

Note that as x approaches $\pm\infty$, $\hat{u}' \to 0$ and $\hat{u} \to u_\pm$ so that

29

$$-s(u_+ - u_-) + \frac{1}{2}(u_+^2 - u_-^2) = 0. \tag{4.6}$$

Equation (4.6) is the Rankine-Hugoniot condition which states that s multiplied by the jump in u denoted $[u] := u_- - u_+$ equals the jump in $\frac{1}{2}u^2$ denoted $[\frac{1}{2}u^2]$. We simplify (4.6) to get

$$s = \frac{u_+ + u_-}{2}. \tag{4.7}$$

Now returning to equation (4.5) and solving for $\hat{u}'$ we obtain

$$\hat{u}' = \frac{1}{2\nu}(\hat{u} - u_-)(\hat{u} - u_+). \tag{4.8}$$

The solution is,

$$\hat{u}(x) = s - a\tanh\left(\frac{a(x - st + \delta)}{2\nu}\right), \tag{4.9}$$

where $a = \frac{1}{2}(u_- - u_+)$.

4.1.1 Evans Function. We first find the eigenvalue problem by changing (4.1) to a scaled moving frame of reference, $(x, t) \to (\frac{x - st + \delta}{v}, \frac{t}{v})$, and find steady-state solutions to the equation

$$u_t - su_x + uu_x = u_{xx}. \tag{4.10}$$

Linearizing about the steady-state solution $\hat{u}$ in (4.10) gives

$$u_t - su_x + \hat{u}u_x + \hat{u}_x u = u_{xx}. \tag{4.11}$$

This yields the eigenvalue problem

$$\lambda u - su' + \hat{u}u' + \hat{u}'u = u''. \tag{4.12}$$

30
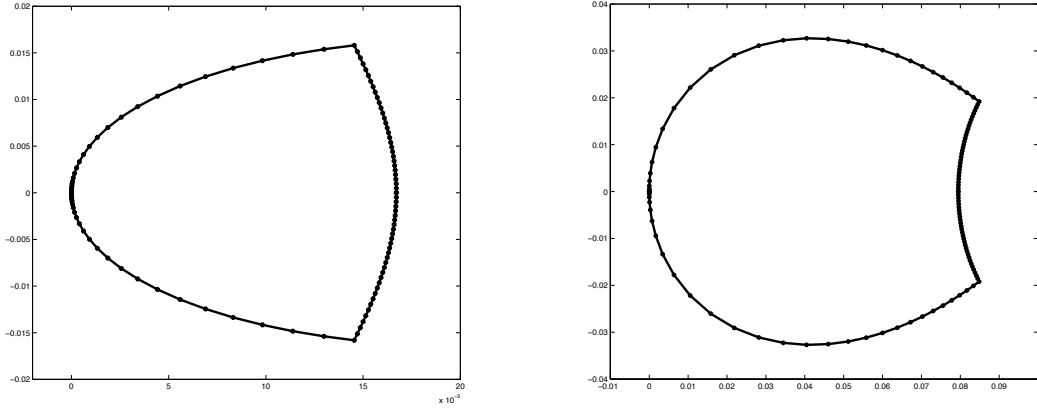
Figure 4.1: Burgers equation Evans function output for a semi-circular contour of radius 10 using 60 mesh points. Numerical infinity is set to $x = 12$. We have (left) $u_- = 10$ and $u_+ = 2$ and (right) $u_- = 4$ and $u_+ = 2$.

We write the eigenvalue problem (4.12) as a first order system,

$$W' = A(x, \lambda)W, \tag{4.13}$$

that is,

$$\begin{pmatrix} u \\ u' \end{pmatrix}' = \begin{pmatrix} 0 & 1 \\ \lambda + \hat{u}' & \hat{u} - s \end{pmatrix} \begin{pmatrix} u \\ u' \end{pmatrix}. \tag{4.14}$$

We use STABLAB to evaluate the Evans function. This yields the output shown in Figure 4.1. Note that the contour goes through $\lambda = 0$ since this is an eigenvalue of (4.12) with corresponding eigenfunction $\hat{u}'$. In A.6 we consider the integrated coordinates case. Excluding the origin yields winding number zero consistent with stability.

4.2 GKDV

Consider the generalized Korteweg-de Vries equation (gKdV), see [39, 38] for details,

$$u_t + u_{xxx} + (1/p)(u^p)_x = 0, \quad p \geq 2, \quad p \in \mathbb{N}. \tag{4.15}$$

31

We look for a traveling pulse solution of the form,

$$\hat{u}(x) = u(x - st, t), \quad \hat{u}^{(n)}(\pm\infty) = 0, \quad n = 0, 1, 2... \tag{4.16}$$

Equivalently we translate $(x, t) \rightarrow (x - st, t)$ and look for stationary solutions of

$$u_t - su_x + u_{xxx} + (u^p/p)_x = 0. \tag{4.17}$$

We may scale out s under the transformation $(u, x, t) \rightarrow (s^{1/(p-1)}u, s^{1/2}x, s^{3/2}t)$ to get

$$u_t - u_x + u_{xxx} + (u^p/p)_x = 0. \tag{4.18}$$

Under the new rescaling, the profile ODE becomes

$$u''' - u' + (u^p/p)' = 0. \tag{4.19}$$

Integrating twice and using separation of variables results in the solution,

$$\hat{u}(x) = \left(\frac{p(p+1)}{2}\right)^{1/(p-1)} \operatorname{sech}((1-p)x/2 + \delta)^{2/(p-1)}, \tag{4.20}$$

where $\delta \in \mathbb{R}$ is some translate. The linearized eigenvalue problem is

$$\lambda u - u' + u''' + (\hat{u}^{p-1}u)' = 0. \tag{4.21}$$

Translating to integrated coordinates $(u \rightarrow u')$ we have

$$\lambda u - u' + u''' + \hat{u}^{p-1}u' = 0. \tag{4.22}$$

We write (4.22) as a first order system,

$$
\begin{pmatrix} u \\ u' \\ u'' \end{pmatrix}' = \begin{pmatrix} 0 & 1 & 0 \\ 0 & 0 & 1 \\ -\lambda & 1 - \hat{u}^{p-1} & 0 \end{pmatrix} \begin{pmatrix} u \\ u' \\ u'' \end{pmatrix}.
\tag{4.23}
$$

Our first order system has a two dimensional growth manifold at $x = -\infty$ and a one dimensional decay manifold at $x = +\infty$. Hence, we use the adjoint formulation of the Evans function at $x = -\infty$ as described in section 2.4. The output in Figure 4.2 has winding number one indicating that the gKdV system is not spectrally stable, which holds anytime $p > 5$; see [39, 38]. We use the winding number and root finding methods discussed in section 3.5 on this system. Table 3.1 demonstrates the effectiveness of the method of moments for finding the root of the Evans function.
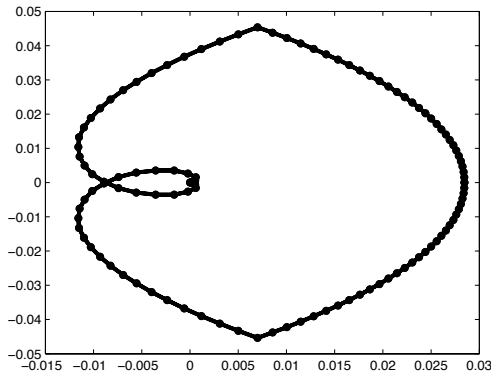
Figure 4.2: Evans function output for the generalized Korteweg-de Vries equation with $p = 7$.

4.3 p-SYSTEM

We consider the p-system with real viscosity, also known as the one dimensional isentropic compressible Navier-Stokes equations, in Lagrangian coordinates,

$$
\begin{aligned}
v_t - u_x &= 0 \\
u_t + p(v)_x &= \left(\frac{u_x}{v} \right)_x,
\end{aligned}
\tag{4.24}
$$

where v is the specific volume, u is the velocity, and $p(v)$ is the pressure law which we assume to be adiabatic satisfying $p(v) = a_0 v^{-\gamma}$, $a_0 > 0$ and $\gamma \geq 1$.

We seek traveling wave solutions to (4.24) with end states $(v_\pm, u_\pm)$, $v_- > v_+ > 0$, by translating $(x, t) \to (x - st, t)$ and considering stationary solutions of

$$v_t - sv_x - u_x = 0$$
$$u_t - su_x + (a_0 v^{-\gamma})_x = \left(\frac{u_x}{v}\right)_x.$$

(4.25)

Rescaling by $(x, t, v, u) \to (-\varepsilon sx, \varepsilon s^2 t, v/\varepsilon, -u/(\varepsilon s))$, where $\varepsilon = v_-$ yields

$$v_t + v_x - u_x = 0,$$
$$u' + (av^{-\gamma})' = \left(\frac{u_x}{v}\right)_x,$$

(4.26)

where $a = a_0 \varepsilon^{-\gamma-1} s^{-2}$.

The profile equation thus satisfies,

$$v' - u' = 0$$
$$u' + (av^{-\gamma})' = \left(\frac{u'}{v}\right)',$$

(4.27)

with boundary conditions $(v(\pm\infty), u(\pm\infty)) = (v_\pm, u_\pm)$. Simplifying gives

$$v' + (av^{-\gamma})' = \left(\frac{v'}{v}\right)'.$$

(4.28)

Integrating from $-\infty$ to x yields the profile equation

$$v' = v(v - 1 + a(v^{-\gamma} - 1)).$$

(4.29)

Setting $x = +\infty$ we find

$$a = -\frac{v_+ - 1}{v_+^{-\gamma} - 1} = v_+^\gamma \frac{1 - v_+}{1 - v_+^\gamma}.$$

(4.30)

34

We linearize (4.26) about the profile $(\hat{v}, \hat{u})$ to find the eigenvalue problem,

$$\lambda v + v' - u' = 0,$$
$$\lambda u + u' - \left(\frac{h(\hat{v})}{\hat{v}^{\gamma+1}} v\right)' = \left(\frac{u'}{\hat{v}}\right)',$$

(4.31)

where $h(\hat{v}) = -\hat{v}^{\gamma+1} + a(\gamma - 1) + (a+1)\hat{v}^{\gamma}$.

Changing to integrated coordinates, $(u, v) \to (u', v')$ we have

$$\lambda v + v' - u' = 0,$$
$$\lambda u + u' - \frac{h(\hat{v})}{\hat{v}^{\gamma+1}} v' = \frac{u''}{\hat{v}}.$$

(4.32)

Writing (4.32) as a first order system yields,

$$A(x, \lambda) = \begin{pmatrix} 0 & \lambda & 1 \\ 0 & 0 & 1 \\ \lambda\hat{v} & \lambda\hat{v} & f(\hat{v}) - \lambda \end{pmatrix}, \quad W = \begin{pmatrix} u \\ v \\ v' \end{pmatrix}, \quad ' = \frac{d}{dx},$$

(4.33)

where $f(\hat{v}) = \hat{v} - \hat{v}^{-\gamma} h(\hat{v})$, with h as before.

Once again using STABLAB, we have in Figure 4.3 the numerical profile and the Evans function output as $v_+ \to 0$. We note that as $v_+ \to 0$ the Evans function approaches a limiting contour. Humpherys, Lafitte, and Zumbrun discovered this limiting behavior numerically which led them to prove stability analytically in the limiting case [24] demonstrating the power of employing the Evans function to study shock wave stability. See also [37] ,[3].

4.4 p-SYSTEM WITH CAPILLARITY

We consider the isentropic gas dynamics system with capillarity (Slemrod's model),

$$v_t - u_x = 0$$
$$u_t + p(v)_x = \left(\frac{u_x}{v}\right)_x - dv_{xxx},$$

(4.34)

Figure 4.3: The profile equation (left) and Evans function output (right) for the p-system as $v_+ \to 0$.

where v is the the specific volume, u is the velocity in Lagrangian coordinates, the constant $d \geq 0$ represents capillarity strength, and $p(v)$ is the pressure law for an ideal gas.

Translating $(x,t) \to (x - st, t)$ we have,

$$
\begin{aligned}
v_t - sv_x - u_x &= 0, \\
u_t - su_x + p(v)_x &= \left(\frac{u_x}{v}\right)_x - dv_{xxx}.
\end{aligned}
\tag{4.35}
$$

Rescaling, $(x, t, u) \to (-sx, s^2 t, -u/s)$ the system becomes

$$
\begin{aligned}
v_t + v_x - u_x &= 0, \\
u_t + u_x + ap(v)_x &= \left(\frac{u_x}{v}\right)_x - dv_{xxx},
\end{aligned}
\tag{4.36}
$$

where $a = 1/s^2$.

The profile equations satisfy

$$
\begin{aligned}
v' - u' &= 0, \\
u' + ap(v)' &= \left(\frac{v'}{v}\right)' - dv''',
\end{aligned}
\tag{4.37}
$$

which simplifies to

$$
v' + ap(v)' = \left(\frac{v'}{v}\right)' - dv'''
\tag{4.38}
$$

36

with boundary conditions $(v, u)(\pm\infty) = (v_\pm, u_\pm)$. Integrating from $-\infty$ to x yields

$$v - v_- + a(p(v) - p(v_-)) = \frac{v'}{v} - dv'', \tag{4.39}$$

where

$$a = -\frac{v_+ - v_-}{p(v_+) - p(v_-)} \tag{4.40}$$

is found by setting $x = +\infty$ to get the Rankine-Hugoniot condition. We take $p(v) = v^{-\gamma}$.

Linearizing (4.36) about the profile equation $(\hat{v}, \hat{u})$ yields the eigenvalue problem

$$\lambda v + v' - u' = 0,$$
$$\lambda u + u' - (f(\hat{v})v)' = \left(\frac{u'}{\hat{v}}\right)' - dv''', \tag{4.41}$$

where $f(\hat{v}) = -ap'(\hat{v}) - \hat{v}_x/\hat{v}^2$. Transforming to integrated coordinates yields,

$$\lambda v + v' - u' = 0,$$
$$\lambda u + u' - f(\hat{v})v' = \frac{u''}{\hat{v}} - dv'''. \tag{4.42}$$

Writing (4.42) as a first order system gives

$$A(x, \lambda) = \begin{pmatrix} 0 & \lambda & 1 & 0 \\ 0 & 0 & 1 & 0 \\ 0 & 0 & 0 & 1 \\ \lambda/d & \lambda/d & h/d & -(d\hat{v})^{-1} \end{pmatrix}, \quad W = \begin{pmatrix} u \\ v \\ v' \\ v'' \end{pmatrix}, \tag{4.43}$$

where $h = h(\hat{v}, \lambda) := 1 + ap'(\hat{v}) + \hat{v}_x/\hat{v}^2 - \lambda/\hat{v}$. There are two growth/decay modes of (4.43) at both $\pm\infty$ making the ODE a stiff problem. We overcome this difficulty by using either the method of continuous orthogonalization or the compound matrix method. To use the compound matrix

method we lift $A(x, \lambda)$ into the exterior product space $\Lambda^2(\mathbb{C}^4) \approx \mathbb{C}^6$ obtaining,

$$
A^{(2)}(x, \lambda) = \begin{pmatrix}
0 & 1 & 0 & -1 & 0 & 0 \\
0 & 0 & 1 & \lambda & 0 & 0 \\
\lambda/d & h/d & -(d\hat{v})^{-1} & 0 & \lambda & 1 \\
0 & 0 & 0 & 0 & 1 & 0 \\
-\lambda/d & 0 & 0 & h/d & -(d\hat{v})^{-1} & 1 \\
0 & -\lambda/d & 0 & -\lambda/d & 0 & -(d\hat{v})^{-1}
\end{pmatrix} ; \qquad (4.44)
$$

see (3.16) and related discussion. We use STABLAB to verify some of the Evans function output given in [23]. First, we numerically solve the profile equations. For small d the solution is monotone, but as capillarity strength increases, the traveling wave becomes oscillatory, as in Figure 4.4. For large capillarity strength, the profile becomes too oscillatory for accurate Evans function results; overcoming this difficulty is an interesting direction for further work. In Figure 4.5 we give some typical Evans function output and in Figure 4.6 we show the affect of varying v_+ and d.
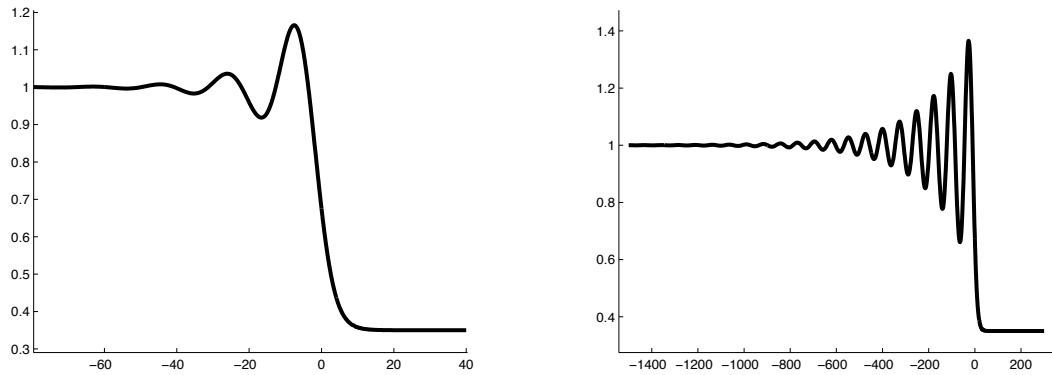
Figure 4.4: The profile equation for the p-system with capillarity. As capillarity strength increases, the profile becomes highly oscillatory.

38
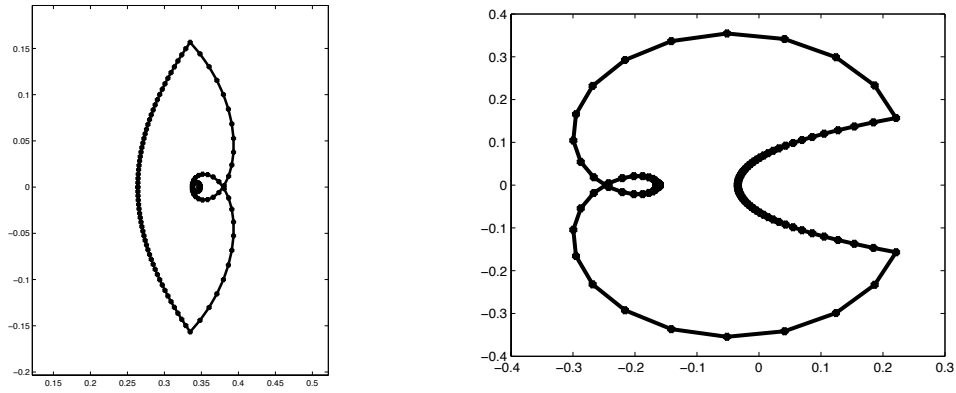
Figure 4.5: Evans function output for the *p*-system with capillarity. Here $d = 0.45$ and $v_+ = 0.65$ (left) and 0.25 (right).
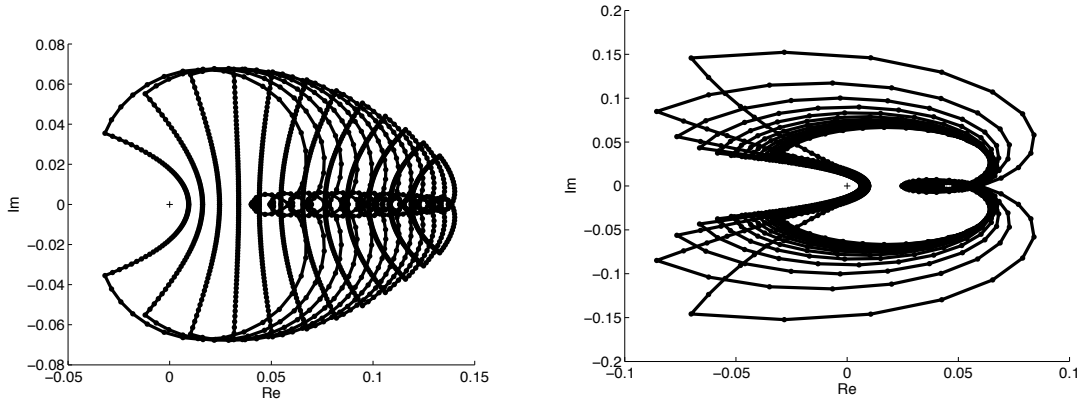
Figure 4.6: Evans function output of a semi-circular contour for the *p*-system with capillarity. On the left $d = 0.75$ and $v_+ \in [0.20, 0.80]$. The contours get closer to the origin and begin to wrap around it as shock strength increases. The contours move away from the origin and shrink in the small shock limit. On the right, $v_+ = 0.25$ and $d \in [0.15, 0.80]$. The contours get larger and more spread out as d decreases.

Chapter 5. Isentropic MHD

In this chapter we discuss the numerical results of our work done in [4] as well as summarize a few of the analytical results.

5.1 Introduction

Consider the system,

$$
\begin{cases}
v_t - u_{1x} = 0 \\
u_{1t} + \left(p + \left(\dfrac{1}{2\mu_0} \right) (B_2^2 + B_3^2) \right)_x = (2\mu + \eta) \left(\dfrac{u_{1x}}{v} \right)_x \\
u_{2t} - \left(\dfrac{1}{\mu_0} B_1^* B_2 \right)_x = \mu \left(\dfrac{u_{2x}}{v} \right)_x \\
u_{3t} - \left(\dfrac{1}{\mu_0} B_1^* B_3 \right)_x = \mu \left(\dfrac{u_{3x}}{v} \right)_x \\
(vB_2)_t - (B_1^* u_2)_x = \left(\left(\dfrac{1}{\sigma \mu_0 v} \right) B_{2x} \right)_x \\
(vB_3)_t - (B_1^* u_3)_x = \left(\left(\dfrac{1}{\sigma \mu_0 v} \right) B_{3x} \right)_x ,
\end{cases}
\tag{5.1}
$$

where v denotes specific volume, $u = (u_1, u_2, u_3)$ velocity, $p = p(v)$ pressure, $B = (B_1^*, B_2, B_3)$ magnetic induction, B_1^* constant, and $\mu > 0$ and $\eta > 0$ the two coefficients of viscosity, $\mu_0 > 0$ the magnetic permeability, and $\sigma > 0$ the electrical resistivity; see [2, 13, 29, 31] for further discussion. With brief exceptions, we take

$$
\eta = -2\mu/3,
\tag{5.2}
$$

as typically prescribed for (nonmagnetic) gas dynamics [5].

By a viscous shock profile of (5.1) we mean a traveling wave solution

$$v(x,t) = \hat{v}(x - st),$$

$$u_1(x,t) = \hat{u}_1(x - st),$$

$$u_2(x,t) = \hat{u}_2(x - st),$$

$$u_3(x,t) = \hat{u}_3(x - st), \tag{5.3}$$

$$(vB_2)(x,t) = \widehat{(vB_2)}(x - st),$$

$$(vB_3)(x,t) = \widehat{(vB_3)}(x - st),$$

moving with speed s and having asymptotically constant end-states
$(v_\pm, u_{1\pm}, u_{2\pm}, u_{3\pm}, (vB_2)_\pm, (vB_3)_\pm)$. Alternatively we translate $x \to x - st$ and consider stationary solutions of

$$
\begin{cases}
v_t - sv_x - u_{1x} = 0 \\[2mm]
u_{1t} - su_{1x} + \left(p + \left(\dfrac{1}{2\mu_0} \right) (B_2^2 + B_3^2) \right)_x = (2\mu + \eta) \left(\dfrac{u_{1x}}{v} \right)_x \\[2mm]
u_{2t} - su_{2x} - \left(\dfrac{1}{\mu_0} B_1^* B_2 \right)_x = \mu \left(\dfrac{u_{2x}}{v} \right)_x \\[2mm]
u_{3t} - su_{3x} - \left(\dfrac{1}{\mu_0} B_1^* B_3 \right)_x = \mu \left(\dfrac{u_{3x}}{v} \right)_x \\[2mm]
(vB_2)_t - s(vB_2)_x - (B_1^* u_2)_x = \left(\left(\dfrac{1}{\sigma\mu_0 v} \right) B_{2x} \right)_x \\[2mm]
(vB_3)_t - s(vB_3)_x - (B_1^* u_3)_x = \left(\left(\dfrac{1}{\sigma\mu_0 v} \right) B_{3x} \right)_x
\end{cases}
\tag{5.4}
$$

Under the rescaling,

$(v, u_1, u_2, u_3, \mu_0, x, t, B_1^*) \to (v/\varepsilon, -u_1/(\varepsilon s), u_2/\varepsilon, u_3/\varepsilon, \varepsilon\mu_0, -\varepsilon sx, \varepsilon s^2 t, -B_1^*/s)$, the system becomes

$$
\begin{cases}
v_t + v_x - u_{1x} = 0 \\[2mm]
u_{1t} + u_{1x} + \left(av^{-\gamma} + \left(\dfrac{1}{2\mu_0 s^2} \right) (B_2^2 + B_3^2) \right)_x = (2\mu + \eta) \left(\dfrac{u_{1x}}{v} \right)_x \\[2mm]
u_{2t} + u_{2x} - \left(\dfrac{1}{\mu_0} B_1^* B_2 \right)_x = \mu \left(\dfrac{u_{2x}}{v} \right)_x \\[2mm]
u_{3t} + u_{3x} - \left(\dfrac{1}{\mu_0} B_1^* B_3 \right)_x = \mu \left(\dfrac{u_{3x}}{v} \right)_x \\[2mm]
(vB_2)_t + (vB_2)_x - (B_1^* u_2)_x = \left(\left(\dfrac{1}{\sigma\mu_0 v} \right) B_{2x} \right)_x \\[2mm]
(vB_3)_t + (vB_3)_x - (B_1^* u_3)_x = \left(\left(\dfrac{1}{\sigma\mu_0 v} \right) B_{3x} \right)_x
\end{cases}
\tag{5.5}
$$

41

where $p(v) = a_0 v^{-\gamma}$ and $a = a_0 \varepsilon^{-\gamma-1} s^{-2}$. We may also remove μ by rescaling, so without loss of generality, $\mu = 1$. Linearizing about the profile $(v, u_1, u_2, u_3, B_1, B_2, B_3) = (\hat{v}, \hat{u}_1, 0, 0, B_1^*, 0, 0)$ we have

$$
\begin{cases}
v_t + v_x - u_{1x} = 0 \\[2mm]
u_{1t} + u_{1x} - a\gamma \left(\hat{v}^{-\gamma-1} v\right)_x = (2\mu + \eta) \left(\dfrac{u_{1x}}{\hat{v}} + \dfrac{\hat{u}_{1x}}{\hat{v}^2} v\right)_x \\[2mm]
u_{2t} + u_{2x} - \dfrac{1}{\mu_0} B_1^*(B_2)_x = \mu \left(\dfrac{u_{2x}}{\hat{v}}\right)_x \\[2mm]
u_{3t} + u_{3x} - \dfrac{1}{\mu_0} B_1^*(B_3)_x = \mu \left(\dfrac{u_{3x}}{\hat{v}}\right)_x \\[2mm]
(\hat{v}B_2)_t + (\hat{v}B_2)_x - B_1^*(u_2)_x = \left(\left(\dfrac{1}{\sigma\mu_0}\right)\dfrac{B_{2x}}{\hat{v}}\right)_x \\[2mm]
(\hat{v}B_3)_t + (\hat{v}B_3)_x - B_1^*(u_3)_x = \left(\left(\dfrac{1}{\sigma\mu_0}\right)\dfrac{B_{3x}}{\hat{v}}\right)_x.
\end{cases}
\tag{5.6}
$$

Note the system is decoupled and that equations 3-6 are two copies of the same system. Stability for the first two equations was demonstrated in great generality in [3, 24] . We make the substitution $\alpha = \hat{v}B_2$ and, dropping the subscripts on u_j and B_j, write the eigenvalue problem,

$$
\begin{cases}
\lambda u + u' - \dfrac{1}{\mu_0} B_1^* B' = \mu \left(\dfrac{u'}{\hat{v}}\right)' \\[3mm]
\lambda \alpha + \alpha' - B_1^* u' = \left(\dfrac{1}{\sigma\mu_0}\right) \left(\dfrac{B'}{\hat{v}}\right)'.
\end{cases}
\tag{5.7}
$$

We make the substitution

$$
\tilde{u}(x) = \int_{-\infty}^{x} u(z)dz, \qquad \tilde{\alpha}(x) = \int_{-\infty}^{x} \alpha(z)dz,
\tag{5.8}
$$

to get

$$
\begin{cases}
\lambda \tilde{u}' + \tilde{u}'' - \dfrac{1}{\mu_0} B_1^* B' = \mu \left(\dfrac{\tilde{u}''}{\hat{v}}\right)' \\[3mm]
\lambda \tilde{\alpha}' + \tilde{\alpha}'' - B_1^* \tilde{u}'' = \left(\dfrac{1}{\sigma\mu_0}\right) \left(\dfrac{B'}{\hat{v}}\right)'.
\end{cases}
\tag{5.9}
$$

Then integrating form $-\infty$ to x we have, suppressing the tilde,

$$\begin{cases} \lambda u + u' - \dfrac{1}{\mu_0} B_1^* B = \mu \left(\dfrac{u''}{\hat{v}} \right) \\[4mm] \lambda \alpha + \alpha' - B_1^* u' = \left(\dfrac{1}{\sigma \mu_0} \right) \left(\dfrac{B'}{\hat{v}} \right), \end{cases}$$ (5.10)

or equivalently,

$$\begin{cases} \lambda u + u' - \dfrac{B_1^* \alpha'}{\mu_0 \hat{v}} = \mu \dfrac{u''}{\hat{v}} \\[4mm] \lambda \alpha + \alpha' - B_1^* u' = \dfrac{1}{\sigma \mu_0 \hat{v}} \left(\dfrac{\alpha'}{\hat{v}} \right)'. \end{cases}$$ (5.11)

Our first orders system is thus

$$\begin{pmatrix} u \\ \mu u' \\ \alpha \\ \frac{\alpha'}{\sigma \mu_0 \hat{v}} \end{pmatrix}' = \begin{pmatrix} 0 & 1/\mu & 0 & 0 \\ \lambda \hat{v} & \hat{v}/\mu & 0 & -\sigma B_1^* \hat{v} \\ 0 & 0 & 0 & \sigma \mu_0 \hat{v} \\ 0 & -B_1^* \hat{v}/\mu & \lambda \hat{v} & \sigma \mu_0 \hat{v}^2 \end{pmatrix} \begin{pmatrix} u \\ \mu u' \\ \alpha \\ \frac{\alpha'}{\sigma \mu_0 \hat{v}} \end{pmatrix}.$$ (5.12)

Recall that $\hat{v}$ satisfies

$$v' = (3/4)v(v - 1 + a(v^{-\gamma} - 1)), \qquad a = v_+^\gamma \frac{1 - v_+}{1 - v_+^\gamma}.$$ (5.13)

Before exhibiting our numerical results, we visit some of the energy estimates done in [4].

5.2 ENERGY ESTIMATES

To help with doing energy estimates, we note a few facts.

Fact 1: Suppose v is a smooth real valued function and w is a smooth complex valued function with the property that $w^{(n)}(\pm \infty) = 0$ for $n = 0, 1, 2, ...$ Then $\mathcal{R}e(\int_{\mathbb{R}} v w \bar{w}') = \mathcal{R}e(\int_{\mathbb{R}} v w' \bar{w}) = \mathcal{R}e(-\frac{1}{2} \int_{\mathbb{R}} v' |w|^2)$.

Proof: If $w = (a + ib)$ then $w \bar{w}' = (a + ib)(a' - ib') = aa' + bb' + i(ba' - ab')$ and $\bar{w} w' =$

43

$(a - ib)(a' + ib') = aa' + bb' + i(ab' - ba') = aa' + bb' - i(ba' - ab')$. Now

$$\int_{\mathbb{R}} vw\bar{w}' = v|w|^2|_{-\infty}^{\infty} - \int_{\mathbb{R}} \bar{w}(v_x w + v w_x)$$
$$= -\int_{\mathbb{R}} v_x |w|^2 - \int_{\mathbb{R}} v\bar{w}w_x. \tag{5.14}$$

Thus,

$$2\mathcal{R}e(\int_{\mathbb{R}} vw\bar{w}') = \mathcal{R}e(-\int_{\mathbb{R}} v_x |w|^2), \tag{5.15}$$

so that

$$\mathcal{R}e(\int_{\mathbb{R}} vw\bar{w}') = \mathcal{R}e(\int_{\mathbb{R}} v\bar{w}w') = -\frac{1}{2}\int_{\mathbb{R}} v_x |w|^2. \tag{5.16}$$

Fact 2: Suppose $w^{(n)}(\pm\infty) = 0$, $n = 0, 1, 2, ...$ Then

$$\int_{\mathbb{R}} w''\bar{w} = -\int_{\mathbb{R}} |w'|^2. \tag{5.17}$$

Proof:

$$\int_{\mathbb{R}} w''\bar{w} = \bar{w}w'|_{-\infty}^{\infty} - \int_{\mathbb{R}} |w'|^2$$
$$= -\int_{\mathbb{R}} |w'|^2. \tag{5.18}$$

Fact 3: Suppose w, u are smooth functions with $w^{(n)} = 0$, $u^{(n)} = 0$ for $n = 0, 1, 2...$ Then $\mathcal{R}e(\int_{\mathbb{R}} w'\bar{u}) = \mathcal{R}e(-\int_{\mathbb{R}} \bar{w}u')$ Proof:

$$\int_{\mathbb{R}} w'\bar{u} = w\bar{u}|_{-\infty}^{\infty} - \int_{\mathbb{R}} w\bar{u}', \tag{5.19}$$

so that

$$\mathcal{R}e\left(\int_{\mathbb{R}} w'\bar{u}\right) = \mathcal{R}e\left(-\int_{\mathbb{R}} w\bar{u}'\right) = \mathcal{R}e\left(\overline{-\int_{-\infty}^{\infty} \bar{w}u'}\right) = \mathcal{R}e\left(-\int_{-\infty}^{\infty} \bar{w}u'\right). \tag{5.20}$$

5.3 Stability for $B_1^* = 0$

For $B_1^* = 0$ the eigenvalue equations become

$$\begin{cases} \lambda u + u' = \mu \dfrac{u''}{\hat{v}}, \\[3mm] \lambda \alpha + \alpha' = \left(\dfrac{1}{\sigma \mu_0 \hat{v}} \right) \left(\dfrac{\alpha'}{\hat{v}} \right)', \end{cases} \tag{5.21}$$

or

$$\begin{cases} \lambda \hat{v} u + \hat{v} u' = \mu u'', \\[3mm] \lambda \hat{v} \alpha + \hat{v} \alpha' = \left(\dfrac{1}{\sigma \mu_0} \right) \left(\dfrac{\alpha'}{\hat{v}} \right)'. \end{cases} \tag{5.22}$$

Taking the real part of the complex L^2-inner product of u against the first equation and α against the second equation yields,

$$\begin{cases} \lambda \displaystyle\int_{\mathbb{R}} \hat{v} |u|^2 + \int_{\mathbb{R}} \hat{v} u' \bar{u} - \mu \int_{\mathbb{R}} u'' \bar{u} = 0, \\[4mm] \lambda \displaystyle\int_{\mathbb{R}} \hat{v} |\alpha|^2 + \int_{\mathbb{R}} \hat{v} \alpha' \bar{\alpha} - \int_{\mathbb{R}} \left(\dfrac{1}{\sigma \mu_0} \right) \left(\dfrac{\alpha'}{\hat{v}} \right)' \bar{\alpha} = 0. \end{cases} \tag{5.23}$$

Then summing the two, using Fact 1 and Fact 2, and integrating by parts, we have,

$$\mathcal{R}e \left(\lambda \int_{\mathbb{R}} \hat{v} \left(|u|^2 + |\alpha|^2 \right) \right) = -\int_{\mathbb{R}} \left(\mu |u'|^2 + \left(\dfrac{1}{\sigma \mu_0 \hat{v}} \right) |\alpha'|^2 \right) + \dfrac{1}{2} \int_{\mathbb{R}} \hat{v}_x \left(|u|^2 + |\alpha|^2 \right) < 0, \tag{5.24}$$

a contradiction for $\mathcal{R}e\lambda \geq 0$ and u, α not identically zero (Recall $v \geq 0$, $v_x \leq 0$).

5.4 Stability for infinite μ_0

In the infinite μ_0 case, the eigenvalue equations are given by,

$$\begin{cases} \lambda u + u' = \mu \dfrac{u''}{\hat{v}} \\[3mm] \lambda \alpha + \alpha' - B_1^* u' = 0. \end{cases} \tag{5.25}$$

The first equation is stable by a simple adjustment to the $B_1^* = 0$ case. Assuming $\mathcal{R}e\lambda \geq 0$,

we have $u \equiv 0$ so that the second equation is

$$\lambda \alpha + \alpha' = 0. \tag{5.26}$$

But this equation is constant coefficient and hence stable ($ce^{-\lambda}$ doesn't satisfy boundary conditions).

5.5 INFINITE σ CASE

In the infinite σ case, the eigenvalue equations are

$$\begin{cases} \lambda u + u' - \dfrac{B_1^* \alpha'}{\mu_0 \hat{v}} = \mu \dfrac{u''}{\hat{v}} \\ \lambda \alpha + \alpha' - B_1^* u' = 0. \end{cases} \tag{5.27}$$

We rewrite this in symmetric form as

$$\begin{cases} \mu_0 \hat{v} \lambda u + \mu_0 \hat{v} u' - B_1^* \alpha' = \mu \mu_0 u'' \\ \lambda \alpha + \alpha' - B_1^* u' = 0. \end{cases} \tag{5.28}$$

Taking the real part of the complex L^2-inner product of u against the first equation and α against the second equation and summing gives,

$$\begin{cases} \displaystyle\int_{\mathbb{R}} \mu_0 \hat{v} \lambda |u|^2 + \int_{\mathbb{R}} \mu_0 \hat{v} u' \bar{u} - \int_{\mathbb{R}} B_1^* \alpha' \bar{u} - \int_{\mathbb{R}} \mu \mu_0 u'' \bar{u} = 0 \\ \displaystyle \lambda \int_{\mathbb{R}} |\alpha|^2 + \int_{\mathbb{R}} \alpha' \bar{\alpha} - \int_{\mathbb{R}} B_1^* u' \bar{\alpha} = 0. \end{cases} \tag{5.29}$$

Summing the two equations and using facts 1-3, we have

$$\mathcal{R}e\lambda \left(\int_{\mathbb{R}} \hat{v} \mu_0 |u|^2 + |\alpha|^2 \right) = -\mu \mu_0 \int_{\mathbb{R}} |u'|^2 + \frac{\mu_0}{2} \int_{\mathbb{R}} \hat{v}_x |u|^2 \leq 0, \tag{5.30}$$

a contradiction for $\mathcal{R}e\lambda \geq 0$ and u not identically zero. If $u \equiv 0$, then we have a constant coefficient system for α which is thus stable.

5.6 Renormalized Evans function

There is a square root singularity in the Evans function when $B_1^* = \sqrt{\mu_0 v_+}$. We remove this singularity by introducing the pair of renormalizations

$$\check{D}(\lambda) := \frac{\left((1 - B_1^*/\sqrt{\mu_0})^2 + 4\lambda(\mu/2 + 1/2\sigma\mu_0)\right)^{1/4}}{\left((1 - B_1^*/\sqrt{\mu_0})^2 + 4(\mu/2 + 1/2\sigma\mu_0)\right)^{1/4}} \frac{\left(v_+/4 + \lambda\right)^{1/4}}{\left(v_+/4 + 1\right)^{1/4}}$$

$$\times \frac{\left((1 - B_1^*/\sqrt{\mu_0 v_+})^2 + 4\lambda(\mu/2v_+ + 1/2\sigma\mu_0 v_+^2)\right)^{1/4}}{\left((1 - B_1^*/\sqrt{\mu_0 v_+})^2 + 4(\mu/2v_+ + 1/2\sigma\mu_0 v_+^2)\right)^{1/4}} D(\lambda) \tag{5.31}$$

and

$$\hat{D}(\lambda) := \frac{\left((1 - B_1^*/\sqrt{\mu_0})^2 + 4\lambda(\mu/2 + 1/2\sigma\mu_0)\right)^{1/4}}{\left((1 - B_1^*/\sqrt{\mu_0})^2 + 4(\mu/2 + 1/2\sigma\mu_0)\right)^{1/4}} D(\lambda). \tag{5.32}$$

From [4] we have,

Theorem 5.1. *On $\Re\lambda \geq 0$, the reduced Evans function D is analytic in λ and continuous in all parameters except at $v_+ = 0$ and $B_1 = \sqrt{\mu_0 v_\pm}$, at which points it exhibits algebraic singularities (blow-up) at $\lambda = 0$. The renormalized Evans functions $\check{D}$ and $\hat{D}$ are analytic in λ and continuous in all parameters except at $(\lambda, v_+) = (0, 0)$.*

In the limit that $v_+ \to 0$, the profile equation reduces to $v' = (3/4)v(v - 1)$ which has solution $\hat{v}_0 = 1/2 - 1/2\tanh(3x/8)$. From [4] we have,

Theorem 5.2. *For σ, μ_0 and B_1^* bounded, the reduced Evans function $D(\lambda)$ converges uniformly on compact subsets of $\{\Re\lambda \geq 0\} \setminus \{0\}$ in the large-amplitude limit $v_+ \to 0$ to a limiting Evans function $D^0(\lambda)$ obtained by substituting $\hat{v}_0$ for $\hat{v}$. Likewise, $\check{D}$ and $\hat{D}$ converge to*

$$\check{D}^0(\lambda) := \frac{\left(1 - B_1^*/\sqrt{\mu_0})^2 + 4\lambda(\mu/2 + 1/2\sigma\mu_0)\right)^{1/4}}{\left(1 - B_1^*/\sqrt{\mu_0})^2 + 4(\mu/2 + 1/2\sigma\mu_0)\right)^{1/4}} \lambda^{1/2} D^0(\lambda) \tag{5.33}$$

and

$$\hat{D}^0(\lambda) := \frac{\left((1 - B_1^*/\sqrt{\mu_0})^2 + 4\lambda(\mu/2 + 1/2\sigma\mu_0)\right)^{1/4}}{\left((1 - B_1^*/\sqrt{\mu_0})^2 + 4(\mu/2 + 1/2\sigma\mu_0)\right)^{1/4}} D^0(\lambda), \tag{5.34}$$

47

each continuous on $\Re\lambda \geq 0$. Moreover, for $B_1^* < \sqrt{\mu_0}$, nonvanishing of $\check{D}^0$ on $\{\Re\lambda > 0\}$ is necessary and nonvanishing of $\check{D}^0$ on $\{\Re\lambda \geq 0\}$ is sufficient for reduced Evans stability (i.e., nonvanishing of $\check{D}$, D on $\{\Re\lambda > 0\}$ for $v_+ > 0$ sufficiently small. For $B_1^* > \sqrt{\mu_0}$, nonvanishing of $\hat{D}^0$ on $\{\Re\lambda > 0\}$ is necessary and nonvanishing of $\hat{D}^0$ on $\{\Re\lambda \geq 0\}$ together with a certain sign condition on $\hat{D}(0)$ is sufficient for reduced Evans stability for $v_+ > 0$ sufficiently small.[1] This sign condition is implied in particular by nonvanishing of $\hat{D}(0)$ on the range

$$\sqrt{\mu_0} \leq B_1^* \leq \sqrt{\mu_0} + \max\left\{\sqrt{\frac{\mu_0}{2}}, \sqrt{\frac{1}{2\sigma}}\right\}. \tag{5.35}$$

Finally, we state a Theorem from [4] which gives a bound on where any unstable eigenvalues, if any exist, can occur. This facilitates a numerical study since we can compute the Evans function on a contour containing the bounded region given below and than use the argument principle from complex analysis.

Theorem 5.3. *Nonstable eigenvalues $\Re\lambda \geq 0$ of (5.12) are confined for $0 < v_+ \leq 1$ to the region*

$$\Re\lambda + |\Im\lambda| < \frac{1}{2}\max\left\{\frac{1}{\mu}, \mu_0\sigma\right\} + (B_1^*)^2\sqrt{\frac{\sigma}{\mu\mu_0}}. \tag{5.36}$$

5.7 NUMERICAL STABILITY RESULTS

For a given amplitude, the analytical results in [4] truncate the computational domain to a compact set, thus allowing for a comprehensive numerical Evans function study patterned after [24, 26], which yields Evans stability in the intermediate parameter range. We then demonstrate Evans stability in the large-amplitude limit by (i) verifying convergence to the limiting Evans functions given in Theorem 5.2 (i.e., checking that convergence has occurred to desired tolerance at the limits of values v_+, λ considered), and (ii) verifying nonvanishing on $\Re\lambda \geq 0$ of the limiting functions $\hat{D}^0$, $\check{D}^0$. These computational results, together with the analytical results in [4], give unconditional stability for all values except for cases where two or more parameters blow up simultaneously. The numerical computations were performed in STABLAB.

When compared to the numerical study for isentropic Navier-Stokes [3, 24], this present system is better conditioned, yet much more computationally taxing since there are more free parameters

---

[1] D, $\hat{D}$ are real-valued for real λ by construction, so that $\text{sgn}\hat{D}(0)$ is well-defined.

to cover, i.e., $(\gamma, v_+, B_1^*, \mu_0, \sigma)$; the isentropic model by contrast has only two parameters (γ, v_+). Since each dimension adds, roughly, an order of magnitude to the runtime, we used parallel computation via MATLAB's parallel computing toolbox. In our main study, we computed along 30,870 semi-circular contours corresponding to the parameter values

$$(\gamma, v_+, B_1^*, \mu_0, \sigma) \in [1.0, 3.0] \times [10^{-5}, 0.8] \times [0.2, 3.8] \times [0.2, 3.8] \times [0.2, 3.8].$$

In every case, the winding number was zero, thus demonstrating Evans stability; see Section 5.8 for more details.

We also carried out a number of small studies to illustrate our analytical work in the limiting fixed-amplitude cases. These are briefly described below and are also given more detail in Section 5.8.
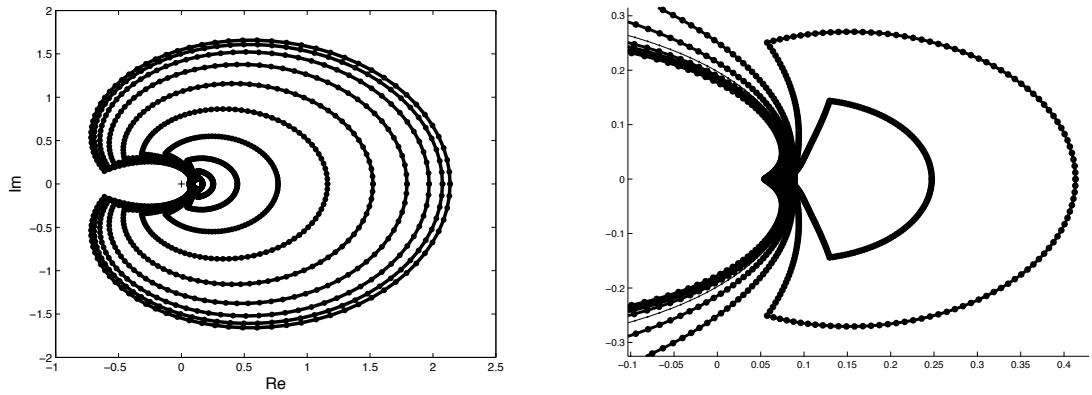
Figure 5.1: Renormalized Evans function output for semi-circular contour of radius 4.5 (left) as the amplitude varies. Parameters are $B_1^* = 2$, $\mu_0 = 1$, $\sigma = 1$, $\gamma = 5/3$, with $v_+ = 10^{-1}, 10^{-1.5}, 10^{-2}, 10^{-2.5}, 10^{-3}, 10^{-3.5}, 10^{-4}, 10^{-4.5}, 10^{-5}, 10^{-5.5}, 10^{-6}$. Note the striking concentric structure of the contours, which converge to the outer contour in the large-amplitude limit (i.e., $v_+ \to 0$) and to a non-zero constant in the small-amplitude limit (i.e., $v_+ \to 1$), indicating stability for all shock strengths since the winding numbers throughout are all zero. The limiting contour given by $\hat{D}^0(\lambda)$ is also displayed, but is essentially identical to nearby contours. When the image is zoomed in near the origin (right), which is marked by a crosshair, we see that the curves are well behaved and distinct from the origin. Also clearly visible is the theoretically predicted square-root singularity at the origin of the limiting contour, as indicated by a right angle in the curve at the image of the origin on the real axis.

In Figure 5.1, we see the typical *concentric* structure as v_+ varies on $[0, 1]$. Note that in the

strong-shock limit, the output converges to the outer contour representing the Evans function output of the limiting system. In the small-amplitude limit, the system converges to a non-zero constant. Since the origin is outside of the contours, one can visually verify that the winding number is zero thus implying Evans stability, even in the strong-shock limit.

In Figure 5.2, we illustrate the convergence of the Evans function as $B_1^* \to \infty$. Note that the contours converge to zero, but they are stable for all finite values of B_1^*. Stability is proven analytically in [4] by a tracking argument.

In Figure 5.3, we see the structure as $\mu_0 \to 0$. Once normalized (right), we see that the structure is essentially unchanged despite a large variation in μ_0; in particular, the shock layers are stable in the $\mu_0 \to 0$ limit. This was proven analytically in [4].

Finally, in Figure 5.4, we see the behavior of the Evans function in the case that $r = \mu/(2\mu + \eta) \to \infty$. This is the opposite case of that considered in [17]. As shown in [4] this case can be computed by disengaging the shooting algorithm and just taking the determinant of initializing e-bases at $\pm\infty$. Notice that in this limit the shock layers are also stable.
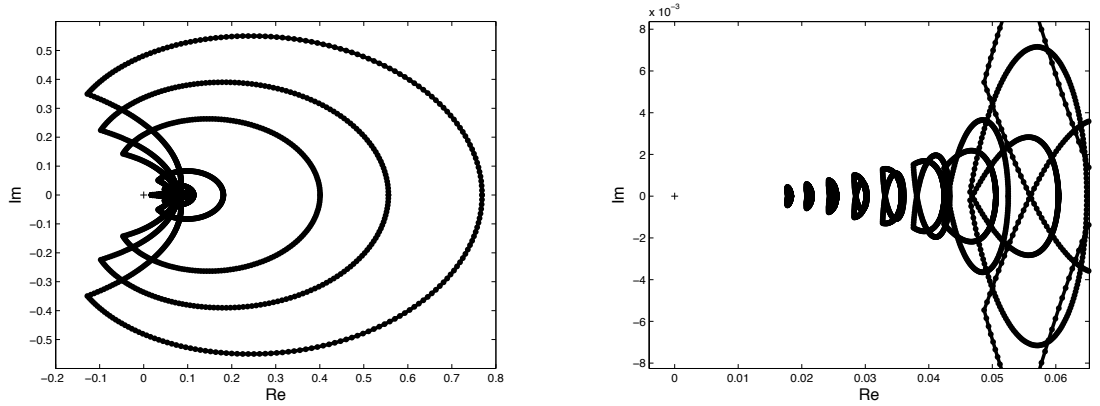
Figure 5.2: Evans function output for semi-circular contour of radius 5 (left) and a zoom-in of the same image near the origin (right). Parameters are $v_+ = 10^{-2}$, $\mu_0 = 1$, $\sigma = 1$, $\gamma = 5/3$, with $B_1^* = 2, 3.5, 5, 10, 15, 20, 25, 30, 35, 40$. Note that the contours converge to zero, which is marked by a cross hair, as $B_1^* \to \infty$.
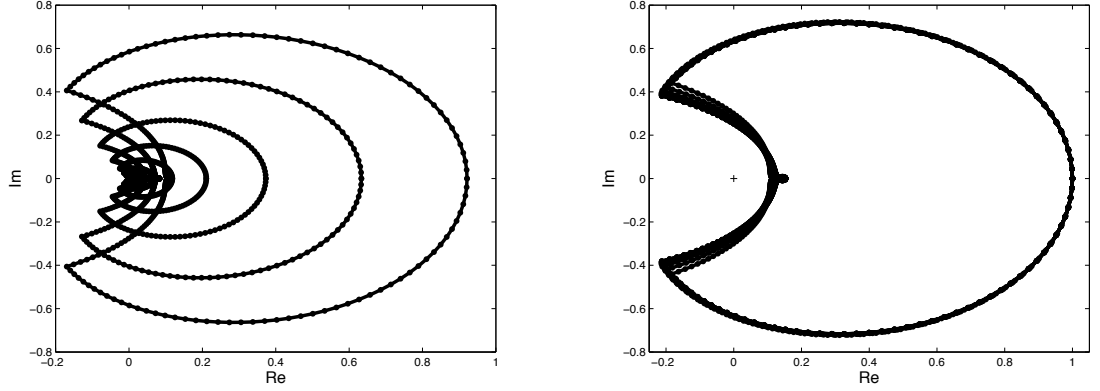
Figure 5.3: Evans function output for semi-circular contour of radius 5 (left) together with a renormalized version of the contours (right), where each contour is divided by its rightmost value, thus putting all contours through $z = 1$ on the right side. Although these results are typical, the parameters in this example are $B_1^* = 2$, $v_+ = 10^{-2}$, $\sigma = 1$, $\gamma = 5/3$, with $\mu_0 = 10^{-.5}, 10^{-1}, 10^{-1.5}, 10^{-2}, 10^{-2.5}, 10^{-3}, 10^{-3.5}, 10^{-4}, 10^{-4.5}, 10^{-5}$. Note that the renormalized contours are nearly identical. This provides a striking indication of stability for all values of μ_0 in our range of consideration, and in particular for $\mu_0 \to 0$.
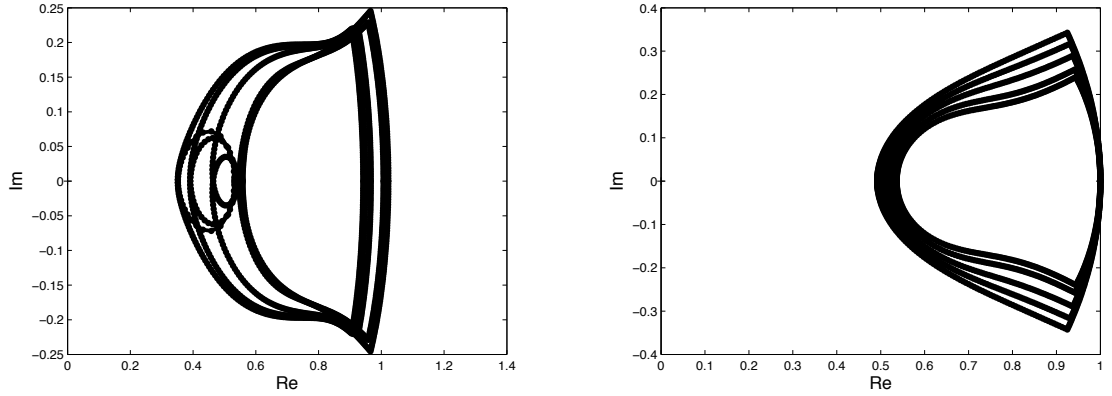
Figure 5.4: Renormalized Evans function in the $r = \infty$ case. Parameters are $v_+ = 10^{-1}$, 10^{-2}, 10^{-3}, 10^{-4}, 10^{-5}, 10^{-6}, $\mu_0 = 1$, $\sigma = 1$, $\gamma = 5/3$. We also have a semi-circular radius of 4.5 with $B_1^* = 2$ (left), and a semi-circular radius of 1 with $B_1^* = 0.5$ (right).

51

5.8 Numerical Investigation

In this section, we discuss our approach to Evans function computation, which is used to determine whether any unstable eigenvalues exist in our system, particularly in the intermediate parameter range left uncovered by analytical results in [4]. Our approach follows the polar-coordinate method developed in [28]; see also [3, 24, 26, 23, 14]. Since the Evans function is analytic in the region of interest, we can numerically compute its winding number in the right-half plane around a large semicircle $B(0, \Lambda) \cap \{\Re \lambda \geq 0\}$ containing (5.36), thus enclosing all possible unstable roots. This allows us to systematically locate roots (and hence unstable eigenvalues) within. As a result, spectral stability can be determined, and in the case of instability, one can produce bifurcation diagrams to illustrate and observe its onset. This approach was first used by Evans and Feroe [16] and has been applied to various systems since; see for example [38, 1, 10, 7].

5.8.1 Approximation of the profile. Following [3, 24], we can compute the traveling wave profile using one of MATLAB's boundary-value solvers `bvp4c` [42], `bvp5c` [32], or `bvp6c` [19], which are adaptive Lobatto quadrature schemes and can be interchanged for our purposes. These calculations are performed on a finite computational domain $[-L_-, L_+]$ with projective boundary conditions $M_\pm(U - U_\pm) = 0$. The values of approximate plus and minus spatial infinity $L_\pm$ are determined experimentally by the requirement that the absolute error $|U(\pm L_\pm) - U_\pm|$ be within a prescribed tolerance, say $TOL = 10^{-3}$; see [26, Section 5.3.4] for a complete discussion. Throughout much of the computation, we used $L_\pm = \pm 20$, but for some rather extreme values in our parameter range, we had to lengthen our interval to maintain good error bounds.

5.8.2 Approximation of the Evans function. Throughout our numerical study, we used the polar-coordinate method described in [28], which encodes $\mathcal{W} = \rho \, \Omega$, where "angle" $\Omega = \omega_1 \wedge \cdots \wedge \omega_k$ is the exterior product of an orthonormal basis $\{\omega_j\}$ of $\mathrm{Span}\{W_1, \ldots, W_k\}$ evolving independently of ρ by some implementation (e.g., Drury's method) of continuous orthogonalization and "radius" ρ is a complex scalar evolving by a scalar ODE slaved to Ω, related to Abel's formula for evolution of a full Wronskian; see [28] for further details. This might be called "analytic orthogonalization", as the main difference from standard continuous orthogonalization routines is that it restores the important property of analyticity of the Evans function by the introduction of the radial function

ρ (Ω by itself is not analytic); see [28, 45] for a discussion on this method.

5.8.3 Shooting and initialization.

The ODE calculations for individual λ are carried out using MATLAB's `ode45` routine, which is the adaptive 4th-order Runge-Kutta-Fehlberg method (RKF45). This method is known to have excellent accuracy with automatic error control. Typical runs involved roughly 300 mesh points per side, with error tolerance set to `AbsTol = 1e-6` and `RelTol = 1e-8`.

To produce analytically varying Evans function output, the initial data $\mathcal{V}(-L_-)$ and $\widetilde{\mathcal{V}}(L_+)$ must be chosen analytically using the method of Kato, see section 3.4. The algorithm of [11] works well for this purpose, as discussed further in [3, 28].

5.8.4 Winding number computation.

We compute the winding number by varying values of λ around the semicircle $B(0, \Lambda) \cap \{\Re\lambda \geq 0\}$ along 120 points of the contour, with mesh size taken quadratic in modulus to concentrate sample points near the origin where angles change more quickly, and summing the resulting changes in $\arg(D(\lambda))$, using $\Im \log D(\lambda) = \arg D(\lambda)(\mathrm{mod}2\pi)$, available in MATLAB by direct function calls. As a check on winding number accuracy, we test a posteriori that the change in argument of D for each step is less than 0.2, and add mesh points, as necessary to achieve this. Recall, by Rouché's Theorem, that accuracy is preserved so long as the argument varies by less than π along each mesh interval.

5.8.5 Description of experiments: broad range.

In our first numerical study, we covered a broad intermediate parameter range to demonstrate stability in the regions not amenable to our analytical results in [4], and also to close our study for unconditional stability for all (finite) system parameters. Since Evans function computation is essentially "embarrassingly parallel", we were able to adapt our STABLAB code to take advantage of MATLAB's parallel computing toolbox, sending to each of 8 "workers" on our 8-core Power Macintosh workstation, different values of λ

producing a net speedup of over 600%. The following parameter combinations were examined:

$$(\gamma, v_+, B_1^*, \mu_0, \sigma) \in \{1.0, 1.1, 11/9, 9/7, 7/5, 5/3, 1.75, 2.0, 2.5, 3.0\}$$
$$\times \{0.8, 0.6, 0.4, 0.2, 10^{-1}, 10^{-2}, 10^{-3}, 10^{-4}, 10^{-5}\}$$
$$\times \{0.2, 0.8, 1.4, 2.0, 2.6, 3.2, 3.8\}$$
$$\times \{0.2, 0.8, 1.4, 2.0, 2.6, 3.2, 3.8\}$$
$$\times \{0.2, 0.8, 1.4, 2.0, 2.6, 3.2, 3.8\}.$$

In total, this is 30,870 contours, each consisting of at least 120 points in λ. In all cases, we found the system to be Evans stable. Typical output is given in Figure 5.1.

We remark that the Evans function is symmetric under reflections along the real axis (conjugation). Hence, we only needed to compute along half of the contour (usually 60 points in the first quadrant) to produce our results.

5.8.6   Description of experiments: limiting parameters.   The purpose of our second study is to verify convergence in the large-amplitude limit $(v_+ \to 0)$, as well as illustrate the analytical results in the limiting cases, namely as $B_1^* \to \infty$, $B_1^* \to 0$, $\mu_0 \to \infty$, $\mu_0 \to 0$, $\sigma \to \infty$, $\sigma \to 0$, $r \to \infty$, and $r \to 0$. In all cases, we found our results to be consistent with stability.

In Table 5.1, we provide typical relative errors between the normalized and limiting-normalized Evans functions in the large-amplitude limit; we varied B_1^* for illustrative purposes. The relative errors are given by computing, respectively,

$$\max_j \left| \frac{\hat{D}(\lambda_j) - \hat{D}^0(\lambda_j)}{\hat{D}^0(\lambda_j)} \right| \quad \text{and} \quad \max_j \left| \frac{\check{D}(\lambda_j) - \check{D}^0(\lambda_j)}{\check{D}^0(\lambda_j)} \right|$$

along the contours except for small λ (that is, when $|\lambda| < 10^{-2}$). Note that in the large-amplitude limit, the relative errors go to zero, as expected.

v_+	$B_1^* = 0.2$	$B_1^* = 0.8$	$B_1^* = 1.4$	$B_1^* = 2$	$B_1^* = 2.6$	$B_1^* = 3.2$	$B_1^* = 3.8$
10(-1)	9.94(-1)	1.23	3.46	9.33	2.16(1)	4.89(1)	1.09(2)
10(-2)	4.36(-1)	5.19(-1)	1.36	2.82	4.92	8.19	1.32(1)
10(-3)	1.42(-1)	1.72(-1)	4.50(-1)	8.34(-1)	1.25	1.86	2.53
10(-4)	4.23(-2)	5.04(-2)	1.32(-1)	2.30(-1)	3.23(-1)	4.55(-1)	5.88(-1)
10(-5)	1.26(-2)	1.50(-2)	4.00(-2)	6.83(-2)	9.35(-2)	1.28(-1)	1.61(-1)
10(-6)	3.94(-3)	4.77(-3)	1.28(-2)	2.18(-2)	2.96(-2)	4.03(-2)	5.01(-2)
10(-7)	2.16(-3)	2.62(-3)	7.08(-3)	1.20(-2)	1.63(-2)	2.21(-2)	2.75(-2)
10(-8)	2.07(-3)	2.51(-3)	6.78(-3)	1.15(-2)	1.56(-2)	2.12(-2)	2.63(-2)

Table 5.1: Relative errors for $\check{D}(\lambda)$ and $\hat{D}(\lambda)$. Here $\sigma = \mu_0 = 0.8$ and $\gamma = 5/3$.

Appendix A. Burgers Equation

A.1   Burgers Equation

Consider Burgers equation,

$$u_t + uu_x = \nu u_{xx} \tag{A.1}$$

where the constant $\nu > 0$ represents viscosity and x and t represent space and time respectively; see [8] for details. Assume that

$$u(x,t) = \hat{u}(x - st) \tag{A.2}$$

where s is wave speed. This substitution reduces the problem to one variable with a moving frame of reference. The solution to this ODE is the wave profile and is stationary because our frame of reference moves along at the same speed as the wave.

We assume asymptotically constant boundary conditions $\hat{u}(\pm\infty) = u_\pm$ where $u_- > u_+$, $\hat{u}(\pm\infty)^{(n)} = 0$, $n = 1, 2, ...$

Transferring $\hat{u}$ into (A.1) we obtain

$$-s\hat{u}' + \hat{u}\hat{u}' = \nu\hat{u}''. \tag{A.3}$$

Integrating yields

$$-s \int_{-\infty}^{x} \hat{u}' + \int_{-\infty}^{x} \hat{u}\hat{u}' = \nu \int_{-\infty}^{x} \hat{u}'', \tag{A.4}$$

which becomes

$$-s(\hat{u} - u_-) + \frac{1}{2}(\hat{u}^2 - u_-^2) = \nu\hat{u}'. \tag{A.5}$$

Note that as x approaches $\pm\infty$, $\hat{u}' \to 0$ and $\hat{u} \to u_\pm$ so that

$$-s(u_+ - u_-) + \frac{1}{2}(u_+^2 - u_-^2) = 0. \tag{A.6}$$

Equation (A.6) is the Rankine-Hugoniot condition which states that s multiplied by the jump in u denoted $[u] := u_- - u_+$ equals the jump in $\frac{1}{2}u^2$ denoted $[\frac{1}{2}u^2]$. We simplify (A.6) to get

$$s = \frac{u_+ + u_-}{2}. \tag{A.7}$$

Now returning to equation (A.5) and solving for $\hat{u}'$ we obtain

$$\hat{u}' = \frac{1}{2\nu}(\hat{u} - u_-)(\hat{u} - u_+). \tag{A.8}$$

The solution is,

$$\hat{u}(x) = s - a\tanh\left(\frac{a(x - st + \delta)}{2\nu}\right), \tag{A.9}$$

where $a = \frac{1}{2}(u_- - u_+)$.

A.2   Numerical Profile

For illustrative purposes, we numerically solve the profile euqation using (A.3) instead of (A.8) allowing us to demonstrate projective boundary conditions. Our boundary value problem does not have a unique solution since a translation is also a solution. Hence, we fix $\hat{u}(0) = s$, the average of our endpoint values. We make the transformation $x \to -x$ on the positive half of the domain thus doubling the dimension of the system. If we let $y_1 = \hat{u}$ and $y_2 = \hat{u}'$ for the left domain and

$y_3 = \hat{u}$ and $y_4 = \hat{u}'$ for the now translated right domain, then the new bvp is

$$
\begin{pmatrix} y_1 \\ y_2 \\ y_3 \\ y_4 \end{pmatrix}' = \begin{pmatrix} y_2 \\ \frac{1}{\nu}(y_1 y_2 - s y_2) \\ y_4 \\ \frac{1}{\nu}(s y_4 - y_3 y_4) \end{pmatrix}, \tag{A.10}
$$

with $y_2(-\infty) = y_4(-\infty) = 0$, $y_1(-\infty) = u_-$, $y_3(-\infty) = u_+$ and $y_1(0) = y_3(0) = s$.

We use projective conditions at $-\infty$ in the bvp solver to scale out the none-growth terms. Let A be the matrix whose columns are the right eigenvectors of the jacobian matrix of the system at $-\infty$. Recall that the left eigenvectors are the rows of A^{-1}. Then if R^g is a right eigenvector corresponding to growth and L^d is a left eigenvector corresponding to none-growth, we have $L^d \cdot R^g = 0$. Then our projective condition is $L^d \cdot (y_{-\infty} - (u_-, 0, u_+, 0)^T)$. Our system has two such projection conditions. This setup causes the boundary value solver to come in orthogonal to the undesired manifold and to fix the solution at $x = -\infty$ at the desired end states. We obtain Figure A.1 using Matlabs `bvp4c` solver. As you can see, reflecting the lower part back to the right side yields the desired tanh solution.
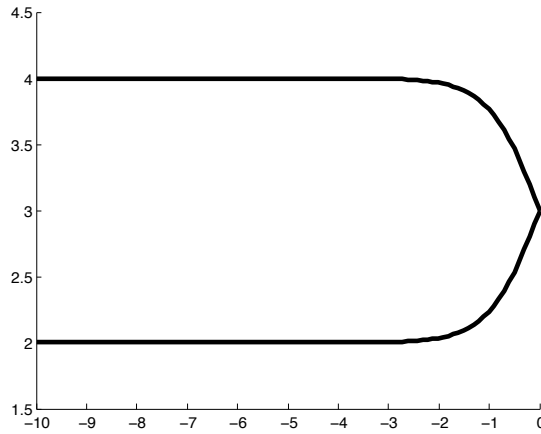
Figure A.1: Traveling Wave Profile

A.3 STABILITY OF BURGERS EQUATION

We say that a traveling wave is spectrally stable if the linearized operator has no eigenvalues in the deleted right half plane, $\{\lambda \in \mathbb{C} \setminus \{0\} \mid \mathbb{R}e(\lambda) \geq 0\}$. Zumbrun and Howard have shown for several general classes of shock waves that spectral stability implies nonlinear stability. We use an energy estimate to prove Burgers equation is spectrally stable.

We first find the eigenvalue problem by changing (A.1) to a scaled moving frame of reference, $(x, t) \rightarrow (\frac{x - st + \delta}{v}, \frac{t}{v})$, and find steady-state solutions to the equation

$$u_t - su_x + uu_x = u_{xx}. \tag{A.11}$$

Linearizing about the steady-state solution $\hat{u}$ in (A.11) gives

$$u_t - su_x + \hat{u}u_x + \hat{u}_x u = u_{xx}. \tag{A.12}$$

This yields the eigenvalue problem

$$\lambda u - su' + \hat{u}u' + \hat{u}'u = u''. \tag{A.13}$$

We make the coordinate change $(u \rightarrow u')$ and then integrate to obtain the integrated eigenvalue problem

$$\lambda u = (s - \hat{u})u' + u''. \tag{A.14}$$

Taking the L^2 inner product with respect to $\bar{u}$, the complex conjugate of u, we obtain

$$\lambda \int_R |u|^2 = \int_R (s - \hat{u})\bar{u}u' + \int_R u''\bar{u}. \tag{A.15}$$

Integrating the right term by parts we have

$$\lambda \int_R |u|^2 = \int_R (s - \hat{u})\bar{u}u' - \int_R |u'|^2. \tag{A.16}$$

Then integrating the middle term by parts we find that $2Re \int (s - \hat{u})\bar{u}u' = \int |u|^2 \hat{u}'$. Note that

58
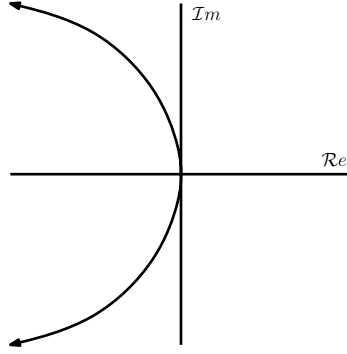
Figure A.2: Essential spectrum of the linearized operator for Burgers equation

$\hat{u}' < 0$. Then

$$Re(\lambda) \int_R |u|^2 = \frac{1}{2} \int_R |u|^2 \hat{u}' - \int_R |u'|^2 < 0 \tag{A.17}$$

so that $Re(\lambda) < 0$. Thus Burgers equation is spectrally stable.

A.4 ESSENTIAL SPECTRUM

Following the discussion in section 2.3.1, we have for (A.13) the Fourier version of the eigenvalue problem,

$$\lambda u = -i\xi A_\pm - B_\pm \xi^2 = \pm i \frac{1}{2}(u_- - u_+)\xi - \xi^2. \tag{A.18}$$

Hence, the essential spectrum is a parabola (see Figure A.2).

A.5 EVANS FUNCTION

Previously we showed stability of traveling wave solutions using energy estimates. Energy estimates often provide a bound on the region in the right half plane where eigenvalues can occur, but do not say whether or not the bounded region contains eigenvalues. Becasue it is analytic, the Evans function may be evaluated on a contour containing the bounded region and the argument principle invoked to determine if there are any eigenvalues inside the contour. We use Burgers Equation to detail how to compute the Evans function.

We write the eigenvalue problem (A.13) as a first order system,

$$W' = A(x, \lambda)W, \tag{A.19}$$

that is,

$$\begin{pmatrix} u \\ u' \end{pmatrix}' = \begin{pmatrix} 0 & 1 \\ \lambda + \hat{u}' & \hat{u} - s \end{pmatrix} \begin{pmatrix} u \\ u' \end{pmatrix}. \tag{A.20}$$

Substituting (A.9) into (A.13) we obtain

$$u'' = \lambda u - a \left(\tanh \left(\frac{ax}{2} \right) u \right)', \tag{A.21}$$

subject to the boundary conditions $u(\pm\infty) = u'(\pm\infty) = 0$.

We are interested in solutions of (A.21) that connect the unstable manifold at $-\infty$ and the stable manifold at $+\infty$. Indeed if the unstable and stable manifold intersect, then λ is an eigenvalue. For simplicity we evaluate the Wronskian at $x = 0$ to check for linear independence.

We begin by using the method of Kato (see section 3.4) to choose analytically varying initial conditions so that the Evans function will be analytic.

The eigenvalues of $A(x, \lambda)$ are

$$\mu_\pm = \frac{\hat{u} - s \mp \sqrt{(\hat{u} - s)^2 + 4(\lambda + \hat{u}')}}{2}, \tag{A.22}$$

which at $x = \pm\infty$ reduce to

$$\mu_\pm = \frac{\mp a \mp \sqrt{a^2 + 4\lambda}}{2}, \tag{A.23}$$

and the associated right and left eigenvectors are

$$r_\pm = v_\pm \begin{pmatrix} 1 \\ \mu_\pm \end{pmatrix}, \qquad l_\pm = \frac{\pm 1}{v_\pm(\mu_- - \mu_+)} \begin{pmatrix} \mu_\mp & -1 \end{pmatrix}, \qquad v_\pm \in \mathbb{C}. \tag{A.24}$$

We obtain our eigenprojection by multiplying the associated stable or unstable right eigenbasis with the left one. This yields the projection,

60

$$P_\pm = r_\pm l_\pm = \frac{\pm 1}{\mu_- - \mu_+} \begin{pmatrix} \mu_\mp & -1 \\ \mu_+ \mu_- & -\mu_\pm \end{pmatrix}.$$

Let $\phi = a^2 + 4\lambda$ so we may simplify to get,

$$P_\pm = \mp \phi^{\frac{-1}{2}} \begin{pmatrix} \mu_\mp & -1 \\ \mu_+ \mu_- & -\mu_\pm \end{pmatrix}$$

so that

$$P'_\pm = \pm 2\phi^{\frac{-3}{2}} \begin{pmatrix} \mu_\mp & -1 \\ \mu_+ \mu_- & -\mu_\pm \end{pmatrix} \mp \phi^{\frac{-1}{2}} \begin{pmatrix} \mp \phi^{\frac{-1}{2}} & 0 \\ -1 & \mp \phi^{\frac{-1}{2}} \end{pmatrix}.$$

Substituting P and P' into the commutator operator and simplifying yields,

$$(P'P - PP')_\pm = \phi^{-1} \begin{pmatrix} -1 & 0 \\ \pm a & 1 \end{pmatrix}.$$

Hence our analytically varying basis satisfies

$$\begin{pmatrix} s'_1 \\ s'_2 \end{pmatrix} = \begin{pmatrix} -\phi^{-1} & 0 \\ \pm a\phi^{-1} & \phi^{-1} \end{pmatrix} \begin{pmatrix} s_1 \\ s_2 \end{pmatrix}.$$

Thus the system of ODEs is

$$\begin{aligned} (s_1^{\pm\infty})' &= \frac{-s_1}{a^2 + 4\lambda} \\ (s_2^{\pm\infty})' &= \frac{\pm a s_1}{a^2 + 4\lambda} + \frac{s_2}{a^2 + 4\lambda} \end{aligned} \qquad (A.25)$$

subject to the initial conditions

$$v_\mp \begin{pmatrix} 1 \\ \mu_\mp \end{pmatrix}.$$

(A.26)

The solution to this system is

$$s_1^{\pm\infty} = k_1^\pm (a^2 + 4\lambda)^{\frac{-1}{4}}$$

$$s_2^{\pm\infty} = k_2^\pm (a^2 + 4\lambda)^{\frac{1}{4}} \mp \frac{a k_1^\pm}{2} (a^2 + 4\lambda)^{\frac{-1}{4}}.$$

(A.27)

From our initial conditions we obtain

$$k_1^\pm = v_\pm (a^2 + 4\lambda_o)^{1/4}$$

$$k_2^\pm = \mp \frac{1}{2} k_1^\pm.$$

(A.28)

Our analytic initializing basis is thus given by (A.27) and (A.28).

Returning now to (A.21),

$$u'' + a \left(\tanh \left(\frac{ax}{2} \right) u \right)' - \lambda u = 0,$$

we see that the general solution is

$$u = C_- \left(\sqrt{4\lambda + a^2} - a \tanh \left(\frac{ax}{2} \right) \right) \operatorname{sech} \left(\frac{ax}{2} \right) \exp \left(\frac{x}{2} \sqrt{4\lambda + a^2} \right)$$

$$+ C_+ \left(-\sqrt{4\lambda + a^2} - a \tanh \left(\frac{ax}{2} \right) \right) \operatorname{sech} \left(\frac{ax}{2} \right) \exp \left(\frac{-x}{2} \sqrt{4\lambda + a^2} \right).$$

For $|x| >> 1$ we have

$$\omega_\pm(x) \approx \begin{pmatrix} u \\ u' \end{pmatrix} = 2C_\pm \begin{pmatrix} \mp(a + \sqrt{4\lambda + a^2}) \\ a^2 + 2\lambda + a\sqrt{4\lambda + a^2} \end{pmatrix} e^{\mp \frac{x}{2}(\sqrt{4\lambda + a^2} + a)}$$

62

Equating this to our initial conditions yields,

$$\mp 2C_\pm(a + \sqrt{4\lambda + a^2}) = s_1 = k_\pm^1(a^2 + 4\lambda)^{-1/4}$$

so that

$$C_\pm = \mp \frac{1}{2} k_\pm^1 \left(a + \sqrt{4\lambda + a^2} \right)^{-1} \left(a^2 + 4\lambda \right)^{-1/4}.$$

Now

$$\omega_\pm(0) = \begin{pmatrix} u \\ u' \end{pmatrix}_{x=0} = C_\pm \begin{pmatrix} \mp\sqrt{4\lambda + a^2} \\ 2\lambda \end{pmatrix}$$

so that

$$D(\lambda) = \begin{vmatrix} u_-(0) & u_+(0) \\ u'_-(0) & u'_+(0) \end{vmatrix} = 4C_-C_+\lambda\sqrt{4\lambda + a^2}.$$

Then substituting for $C_\pm$ the Evans Function is

$$D(\lambda) = \frac{-\lambda k_+^1 k_-^1}{\left(a + \sqrt{4\lambda + a^2} \right)^2}.$$

We note that the Evans Function is analytic in the right half plane and that the only zero is $\lambda = 0$.

A.6 INTEGRATED COORDINATES

Since $\hat{u}$ is a solution of (A.3), we have

$$s\hat{u}' - \hat{u}\hat{u}' + \nu\hat{u}'' = 0.$$

63

Differentiating we have

$$s\hat{u}' - \hat{u}\hat{u}'' - (\hat{u}')^2 + \nu\hat{u}''' = 0.$$

That is, substituting $\hat{u}'$ for u in

$$L(u) = su' - (\hat{u}u)' + u'' \tag{A.29}$$

gives $L(\hat{u}') = 0$ so that $\hat{u}'$ is an eigenvector with eigenvalue 0. This is the eigenvalue associated with translational invariance discussed in section 2.3.

A useful technique for computing the Evans function involves changing the eigenvalue problem to integrated coordinates. Doing so removes the eigenvalue at zero associated with translational invariance while all other eigenvalues remain the same. This both makes it more probable to find uniform bounds when doing energy estimates and aids in numerical computation of the Evans Function. We employ this technique to Burgers Equation along with the method of Kato to see how it simplifies the Evans Function.

Recall that the eigenvalue problem is

$$\lambda u - su' + (\hat{u}u)' = u''. \tag{A.30}$$

We make the coordinate change $(u \to u')$ and then integrate to obtain the integrated eigenvalue problem

$$u'' + (s - \hat{u})u' - \lambda u = 0. \tag{A.31}$$

The ODE is thus

$$\begin{pmatrix} u \\ u' \end{pmatrix}' = \begin{pmatrix} 0 & 1 \\ \lambda & \hat{u} - s \end{pmatrix} \begin{pmatrix} u \\ u' \end{pmatrix}. \tag{A.32}$$

Recall that when we use the method of Kato to find an analytically varying basis for our initial conditions that $x = \pm\infty$. Since $u'(\pm\infty) = 0$, our basis for the integrated problem will be the same as we found previously, that is (A.27).

Now substituting (A.9) into (A.31) we obtain

$$u'' + a \tanh\left(\frac{ax}{2}\right)u' - \lambda u \tag{A.33}$$

which has solution

$$u(x) = c_+ e^{\frac{-x}{2}\sqrt{4\lambda+a^2}}\operatorname{sech}\left(\frac{ax}{2}\right) + \frac{c_-}{\sqrt{4\lambda+a^2}}e^{\frac{x}{2}\sqrt{4\lambda+a^2}}\operatorname{sech}\left(\frac{ax}{2}\right). \tag{A.34}$$

For $x \gg 1$ we have

$$2c_+ \begin{pmatrix} 1 \\ -\frac{1}{2}(a + \sqrt{4\lambda + a^2}) \end{pmatrix} e^{\frac{-x}{2}(\sqrt{4\lambda+a^2}+a)}, \tag{A.35}$$

and for $x \ll 1$ we have

$$\frac{2c_-}{\sqrt{4\lambda+a^2}} \begin{pmatrix} 1 \\ \frac{1}{2}(a + \sqrt{4\lambda + a^2}) \end{pmatrix} e^{\frac{x}{2}(\sqrt{4\lambda+a^2}+a)}. \tag{A.36}$$

Then

$$\begin{aligned} c_+ &= \frac{1}{2}k_1^+(a^2 + 4\lambda)^{\frac{-1}{4}} \\ c_- &= \frac{1}{2}k_1^-(a^2 + 4\lambda)^{\frac{1}{4}}. \end{aligned} \tag{A.37}$$

Now

$$w_+(0) = c_+ \begin{pmatrix} 1 \\ \frac{-1}{2}\sqrt{4\lambda + a^2} \end{pmatrix} \tag{A.38}$$

and

$$w_-(0) = \frac{c_-}{2} \begin{pmatrix} \frac{2}{\sqrt{4\lambda+a^2}} \\ 1 \end{pmatrix}. \tag{A.39}$$

Hence

65

$$\begin{vmatrix} w_-(0) & w_+(0) \end{vmatrix} = -c_+c_-. \tag{A.40}$$

Then

$$D(\lambda) = -\frac{1}{4}k_1^+ k_1^- = \text{constant}. \tag{A.41}$$

We see that using the integrated coordinate transformation and the method of Kato has greatly simplified the Evans Function.

Appendix B. Exterior Products

Let V be a finite dimensional vector space over the field of scalars F. Let $W_k = V \times V \times \dots \times V$ denote the product set $\{(v_1, v_2, \dots, v_k)|v_i \in V\}$. Let $F(W_k)$ be the set consisting of all finite linear combinations of elements of W_k. That is, an element of $F(W_k)$ takes the form $\sum_{j=1}^{M} \alpha_j V_j$ where $\alpha_j \in F$ and $V_j \in W_k$. Let $S(W_k)$ be the subset of $F(W_k)$ generated by the set of all elements of the following types:

$$(u_1, .., w + v, .., u_k) - (u_1, .., w, .., u_k) - (u_1, .., v, .., u_k)$$

$$(u_1, .., \alpha u_p, .., u_k) - \alpha(u_1, .., u_p, .., u_k) \quad \alpha \in F$$

$$(u_1, u_2, .., u_k) \quad u_i = u_j \text{ for some } i \neq j$$

Define $\bigwedge^k V$ to be the quotient space $F(W_k)/S(W_k)$, and define $u_1 \wedge \dots \wedge u_k = [(u_1, \dots, u_k)]$ = equivalence class of $(u_1, \dots, u_k)$. Thus two vectors are equivalent if their difference is in $S(W_k)$. Note that $F(W_k)/S(W_k)$ forms a vector space. We call $\bigwedge^k V$ the k-th exterior power of V and a vector in $\bigwedge^k V$ is called a k-vector or k-form. Using our new notation we have the following properties,

$$u_1 \wedge \dots \wedge (\alpha w + \beta v) \wedge \dots \wedge u_k = \alpha(u_1 \wedge \dots \wedge w \wedge \dots \wedge u_k) + \beta(u_1 \wedge \dots \wedge v \wedge \dots \wedge u_k), \tag{B.1}$$

and

$$u_1 \wedge ... \wedge u_k = 0 \qquad \text{whenever } u_i = u_j \text{ for } i \neq j. \tag{B.2}$$

Lemma B.1. *The following holds:*

$$u_1 \wedge ... \wedge u_q \wedge ... \wedge u_p \wedge ... \wedge u_k = -u_1 \wedge ... \wedge u_p \wedge ... \wedge u_q \wedge ... \wedge u_k.$$

Proof. By property (B.2) we have

$$u_1 \wedge ... \wedge (v + w) \wedge ... \wedge (v + w) \wedge ... \wedge u_k = 0.$$

Expanding as in (B.1) we obtain,

$$0 = u_1 \wedge ... \wedge v \wedge ... \wedge v \wedge ... \wedge u_k$$
$$+ u_1 \wedge ... \wedge v \wedge ... \wedge w \wedge ... \wedge u_k$$
$$+ u_1 \wedge ... \wedge w \wedge ... \wedge v \wedge ... \wedge u_k$$
$$+ u_1 \wedge ... \wedge w \wedge ... \wedge w \wedge ... \wedge u_k.$$

Two terms cancel using property (B.2) so that

$$u_1 \wedge ... \wedge v \wedge ... \wedge w \wedge ... \wedge u_k = -u_1 \wedge ... \wedge w \wedge ... \wedge v \wedge ... \wedge u_k. \qquad \square$$

$\square$

Definition B.2. A permutation π is a bijective map from $[1, 2, ..., m]$ to itself. We denote the set of permutations defined on $[1, 2, ..., m]$ by P_m and use $\pi(k)$ to represent the image of k under π.

Proposition B.3. *Let $\{v_1, ..., v_n\}$ form a basis for V. Then the k-vectors of the form*

$$\{v_{\pi(1)} \wedge ... \wedge v_{\pi(k)} | 1 \leq \pi(1) < ... < \pi(k) \leq n\}$$

form a basis for $\bigwedge^k V$.

Proof. Any k-form in $\bigwedge^k V$ can be written

$$\sum_{r=1}^{M} u_{r,1} \wedge u_{r,2} \wedge ... \wedge u_{r,k}, \tag{B.3}$$

where $u_{r,j} \in V$ and $M \in \mathbb{N}$. Expanding $u_{r,j}$ in terms of $\{v_i\}$ yields

$$\sum_{r=1}^{M} (\alpha_{r,1,1}v_1 + ... + \alpha_{r,1,n}v_n) \wedge ... \wedge (\alpha_{r,k,1}v_1 + ... + \alpha_{r,k,n}v_n). \tag{B.4}$$

Repeated use of property (B.2) and Lemma B.1 yields the linear combination,

$$\sum_{\pi \in P} \beta_\pi v_{\pi(1)} \wedge ... \wedge v_{\pi(k)}.$$

$\square$

Definition B.4. Let W be a vector space. A map $L : W_k \to W$ is **multilinear** if $L(u_1, .., \alpha u_p + \beta \tilde{u}_p, .., u_k) = \alpha L(u_1, .., u_p, .., u_k) + \beta L(u_1, .., \tilde{u}_p, .., u_k)$ for $p = 1, 2, ...k$. The map L is *alternating* or *antisymmetric* if $L(u_{\pi(1)}, ..., u_{\pi(k)}) = \text{sign}(\pi) L(u_1, ..., u_k)$, $\pi \in P_k$.

Theorem B.5 (Universal Alternating Mapping Property). *If $L : W_k \to W$ is a multilinear alternating map, then there exists a unique linear map*
$\hat{L} : \bigwedge^k V \to W$ *such that* $\hat{L}(u_1 \wedge ... \wedge u_k) = L(u_1, ..., u_k)$, $\forall u_1, ..., u_k$.

Proof. A multilinear alternating map $L : W_k \to W$ is uniquely extended to a linar map $\bar{L} : F(W_k) \to W$ by defining

$$\bar{L}\left(\sum_{j=1}^{M} \alpha_j V_j\right) = \sum_{j=1}^{M} \alpha_j L(V_j),$$

where $\alpha_j \in F$ and $V_j \in W_k$. Note that $S(W_k)$ is in the kernel of $\bar{L}$. Consequently, every $\phi \in F(W_k)$ in the equivalence class $[\phi] \in \bigwedge^k V$ maps to the same element $\bar{L}(\phi)$ in W. Define $\hat{L}([\phi]) = \bar{L}(\phi)$. That is

$$\hat{L}(u_1 \wedge ... \wedge u_k) = \hat{L}([(u_1, ..., u_k)]) = L(u_1, ..., u_k).$$

Suppose $\tilde{L}$ were another such map. Then

$$\tilde{L}(u_1 \wedge ... \wedge u_k) = \hat{L}(u_1 \wedge ... \wedge u_k), \ \forall(u_1, ..., u_k),$$

so that $\tilde{L} - \hat{L}$ is zero on the generators of $\bigwedge^k V$, and thus on all of $\bigwedge^k V$. $\qquad\square$

Definition B.6. If V is a vector space over F where $F = \mathbb{R}$ or $F = \mathbb{C}$, an **inner product** on V is a function $\langle \cdot, \cdot \rangle : V \times V \to F$ which for all $\alpha, \beta \in F$ and for all $x, y, z \in V$ satisfies:

   (i) $\langle \alpha x + \beta y, z \rangle = \alpha \langle x, z \rangle + \beta \langle y, z \rangle$,

   (ii) $\langle x, \alpha y + \beta z \rangle = \bar{\alpha} \langle x, y \rangle + \bar{\beta} \langle x, z \rangle$,

   (iii) $\langle x, x \rangle \geq 0$ and $\langle x, x \rangle = 0 \Rightarrow x = 0$

   (iv) $\langle x, y \rangle = \overline{\langle y, x \rangle}$.

Definition B.7. A k-form in $\bigwedge^k V$ is called a **pure form** if it is a wedge product between k linearly independent vectors in V. A k-form is **decomposable** if it can be written as a pure form.

Note that every element of $\bigwedge^k V$ is a sum of decomposable elements.

Theorem B.8. *Let V be a vector space with inner product $\langle \cdot, \cdot \rangle$. Then*

$$[u, v] := \det \begin{pmatrix} \langle u_1, v_1 \rangle & \cdots & \langle u_1, v_k \rangle \\ \vdots & \ddots & \vdots \\ \langle u_k, v_1 \rangle & \cdots & \langle u_k, v_k \rangle \end{pmatrix} \tag{B.5}$$

defined on decomposable elements $u, v \in \bigwedge^k V$ defines an inner product on $\bigwedge^k V$ by extending bilinearly to any k-form.

Proof. Let $\hat{u}, \hat{v}$ represent pure k-forms associated with $u, v \in W_k$. Let λ, μ represent k-forms with

$\lambda = \sum_{j=1}^{n} \alpha_j \hat{u}_j$, $\mu = \sum_{i=1}^{m} \beta_i \hat{v}_i$ where the $\hat{u}_j$, $\hat{v}_i$ are pure k-forms and $\alpha_j, \beta_i \in F$. Define

$$H(u,v) = \det \begin{pmatrix} \langle u_1, v_1 \rangle & \cdots & \langle u_1, v_k \rangle \\ \vdots & \ddots & \vdots \\ \langle u_k, v_1 \rangle & \cdots & \langle u_k, v_k \rangle \end{pmatrix}.$$

Fix $v_0 = (v_1, ..., v_k)$ and $\hat{v}_0 = v_1 \wedge ... \wedge v_k$. Now $H(u, v_0) : W_k \to F$ is alternating and multilinear. By the Universal Alternating Mapping Property, there exists a unique linear map $f_{v_0} : \bigwedge^k V \to F$ such that $f_{v_0}(\hat{u}) = H(u, v_0)$. Fix $\lambda \in \bigwedge^k V$. Now $f_{v_0}(\lambda) = \sum_{j=1}^{n} \alpha_j f_{v_0}(\hat{u}_j) = \sum_{j=1}^{n} \alpha_j H(u_j, v_0)$. Now $H_\lambda(v) := \sum_{j=1}^{n} \alpha_j H(u_j, v)$ is multilinear and alternating, so by the Universal Alternating Mapping Property, there exists a unique linear map $g_\lambda : \bigwedge^k V \to F$ such that $g_\lambda(\hat{v}) = H_\lambda(v)$. Set

$$\begin{aligned} [\lambda, \mu] &:= g_\lambda(\mu) \\ &= \sum_{i=1}^{m} \beta_i g_\lambda(\hat{v}_i) \\ &= \sum_{i=1}^{m} \beta_i H_\lambda(v_i) \\ &= \sum_{i=1}^{m} \beta_i \sum_{j=1}^{n} \alpha_j H(u_j, v_i) \\ &= \sum_{j=1}^{n} \sum_{i=1}^{m} \alpha_j \beta_i H(u_j, v_i). \end{aligned}$$

$\square$

Appendix C. STABLAB Code

In this appendix we document STABLAB.

C.1 Burger's equation

```
function Burgers

beep off; clc; clear all; close all

tic


p.ul=10;

p.ur=2;


%structure variables

s.I=12;


c.ksteps=30;

c.basisL=@analytic_basis;

c.basisR=@analytic_basis;

c.evans=@evans;

c.LA=@A;

c.RA=@A;

c.epsl=0;

c.epsr=0;

c.proj=@projection2;


m.n=2;

e.kl=1;

e.kr=1;

e.evans='reg_reg_polar';


m.damping=0;

m.method=@drury;

m.options=odeset('RelTol',1e-6,'AbsTol',1e-8,'Refine',1,'Stats','on');
```

```
%dependent structure variables
s.R=s.I;
s.L=-s.I;
e.LA=c.LA;
e.RA=c.RA;
e.Li=[s.L 0];
e.Ri=[s.R 0];
c.L=s.L;
c.R=s.R;


%preimage contour
circpnts=30; imagpnts=30; r=10; spread=4; zerodist=10^(-4);
preimage=semicirc(circpnts,imagpnts,c.ksteps,r,spread,zerodist);


halfw=contour(c,s,p,m,e,preimage);
w = [halfw fliplr(conj(halfw))];
wnd=winding_number(w);
plot(w,'-*k');


time=toc;
fprintf('Time: %1.2d seconds\n',time);
fprintf('Winding Number: %1.1d\n',wnd);


function out = A(x,lambda,s,p)


a=.5*(p.ul-p.ur);
cc=.5*(p.ul+p.ur);
u=cc-a*tanh(a*x/2);
uder=(-a^2/2)*sech(a*x/2)^2;
```

```
out=[0 1; lambda+uder u-cc];

function out = Aadj(x,lambda,s,p)


a=.5*(p.ul-p.ur);
cc=.5*(p.ul+p.ur);
u=cc-a*tanh(a*x/2);
uder=(-a^2/2)*sech(a*x/2)^2;


out=-[0 1; lambda+uder u-cc]';
```

C.2   ISENTROPIC

```
function isentropic
beep off; clc; clear all; close all
tic


global s p


%independent variables
p.gamma=5/3;
p.vp=.001;
%dependpent variables
p.a=-(1-p.vp)/(1-p.vp^-p.gamma);


%structure variables
s.I=12;
s.larray=2;
s.rarray=1;
s.side=1;
```

```
c.ksteps=30;

c.basisL=@analytic_basis;

c.basisR=@analytic_basis;

c.evans=@evans;

c.LA=@A;

c.RA=@Aadj;

c.epsl=0;

c.epsr=0;

c.proj=@projection2;


m.n=3;

e.kl=1;

e.kr=1;

e.evans='reg_adj_polar';


m.damping=0;

m.method=@drury;

m.options=odeset('RelTol',1e-6,'AbsTol',1e-8,'Refine',1,'Stats','on');


%dependent structure variables

s.R=s.I;

s.L=-s.I;

e.LA=c.LA;

e.RA=c.RA;

e.Li=[s.L 0];

e.Ri=[s.R 0];

c.L=s.L;

c.R=s.R;

s.sol = getprofile;
```

```
%preimage contour

circpnts=30; imagpnts=30; r=10; spread=4; zerodist=10^(-4);

preimage=semicirc(circpnts,imagpnts,c.ksteps,r,spread,zerodist);


halfw=contour(c,s,p,m,e,preimage);

w = [halfw fliplr(conj(halfw))];

wnd=winding_number(w);

plot(w,'-*k');


time=toc;

fprintf('Time: %1.2d seconds\n',time);

fprintf('Winding Number: %1.1d\n',wnd);

% %%%%%%%%%%%%%%%%%%%%%%%%%%%%%%%%%%%%%%%%%%%%%%%%%%%%%%%

%%%%%%%%%%%%%%%%%%%%%%%%%%%%%%%%%%%%%%%%%%%%%%%%%%%%%%%

function sol = getprofile

global s

% BVP solver


options = bvpset('RelTol', 1e-6, 'AbsTol', 1e-8,'Nmax', 20000);

solinit = bvpinit(linspace(0,s.R,20),@guess);

sol = bvp5c(@double_F,@bc,solinit,options);


%%%%%%%%%%%%%%%%%%%%%%%%%%%%%%%%%%%%%%%%%%%%%%%%%%%%%%%

function out = guess(x)

global s p

a = 0.5*(1+p.vp);

c = 0.5*(1-p.vp);

out = [a-c*tanh((s.R/s.I)*x);a-c*tanh((s.L/s.I)*x)];
```

```
%%%%%%%%%%%%%%%%%%%%%%%%%%%%%%%%%%%%%%%%%%%%%%%%%%
function out = bc(ya,yb)
global p

out = [ya(1,:)-ya(2,:);
    ya(1) - 0.5*(1+p.vp)];
%%%%%%%%%%%%%%%%%%%%%%%%%%%%%%%%%%%%%%%%%%%%%%%%%%
function out = F(x,v)
global p

out=v*(v-1+p.a*(v^(-p.gamma)-1));

function out = A(x,lambda,s,p)


a=p.a;
gamma=p.gamma;


v=soln(x,s);


out = [0          lambda    1;
       0          0         1;
       lambda*v lambda*v f(v,gamma,a)-lambda];


function out=f(v,gamma,a)
out=v-v^(-gamma)*h(v,gamma,a);


function out=h(v,gamma,a)
out= -v^(gamma+1)+a*(gamma-1)+(a+1)*v^(gamma);atim}


function out = Aadj(x,lambda,s,p)
```

```
a=p.a;
gamma=p.gamma;


v=soln(x,s);


out = -[0          lambda    1;
        0          0         1;
        lambda*v lambda*v f(v,gamma,a)-lambda]';


function out=f(v,gamma,a)
out=v-v^(-gamma)*h(v,gamma,a);


function out=h(v,gamma,a)
out= -v^(gamma+1)+a*(gamma-1)+(a+1)*v^(gamma);
```

C.3   CAPILLARITY

```
function capillarity
beep off; clc; clear all; close all
tic


global s p b


p.d=-.45;
p.gamma=1.4;
p.vp=.15;
p.a=-(1-p.vp)/(1-p.vp^-p.gamma);
p.ul=[1;0];
p.ur=[p.vp;0];
```

```matlab
%structure variables
s.I=25;
s.larray=[3;4];
s.rarray=[1;2];
s.side=1;


c.ksteps=30;
c.basisL=@analytic_basis;
c.basisR=@analytic_basis;
c.evans=@evans;
c.LA=@A;
c.RA=@A;
c.epsl=0;
c.epsr=0;
c.proj=@projection2;


m.n=4;
e.kl=2;
e.kr=2;
e.evans='reg_reg_polar';


m.damping=0;
m.method=@drury;
m.options=odeset('RelTol',1e-6,'AbsTol',1e-8,'Refine',1,'Stats','on');


%dependent structure variables
s.R=s.I;
s.L=-s.I;
e.LA=c.LA;
e.RA=c.RA;
```

```
e.Li=[s.L 0];

e.Ri=[s.R 0];

c.L=s.L;

c.R=s.R;


AM = Flinear(p.ul);

eig(AM)

PM = projection1(AM,-1);

b.LM = orth(PM.').';



AP = Flinear(p.ur);

PP = projection1(AP,1);

b.LP = orth(PP.').';


s.sol = getprofile2;


%preimage contour

circpnts=30; imagpnts=30; r=10; spread=2; zerodist=10^(-2);

preimage=semicirc(circpnts,imagpnts,c.ksteps,r,spread,zerodist);


halfw=contour(c,s,p,m,e,preimage);

w = [halfw fliplr(conj(halfw))];

wnd=winding_number(w);

plot(w,'-*k');


time=toc;

fprintf('Time: %1.2d seconds\n',time);

fprintf('Winding Number: %1.1d\n',wnd);

%%%%%%%%%%%%%%%%%%%%%%%%%%%%%%%%%%%%%%%%%%%%%%%%%%%%%%%%
```

```matlab
function sol = getprofile2
global s
% BVP solver

options = bvpset('RelTol', 1e-6, 'AbsTol', 1e-8,'Nmax', 20000);
solinit = bvpinit(linspace(0,s.I,400),@guess2);
sol = bvp5c(@double_F,@bc2,solinit,options);
%%%%%%%%%%%%%%%%%%%%%%%%%%%%%%%%%%%%%%%%%%%%%%%%%%%%%%%
function out = guess2(x)
global s p
a = 0.5*(p.ul(1)+p.ur(1));
c = 0.5*(p.ul(1)-p.ur(1));

alpha = 0.75;
out = [a-c*tanh(alpha*(s.R/s.I)*x);-c*a*alpha*sech(alpha*(s.R/s.I)*x).^2;...
       a-c*tanh(alpha*(s.L/s.I)*x);-c*a*alpha*sech(alpha*(s.L/s.I)*x).^2;];
%%%%%%%%%%%%%%%%%%%%%%%%%%%%%%%%%%%%%%%%%%%%%%%%%%%%%%%
function out = bc2(ya,yb)
global s b p

out = [ya(s.rarray,:)-ya(s.larray,:);
    ya(1) - 0.5*(p.ul(1)+p.ur(1));
    [b.LP zeros(size(b.LP))] * (yb - [p.ur;p.ul]);
    [zeros(size(b.LM)) b.LM] * (yb - [p.ur;p.ul])];
%%%%%%%%%%%%%%%%%%%%%%%%%%%%%%%%%%%%%%%%%%%%%%%%%%%%%%%
function out = Flinear(U)
global p

out = [0 1;(1+p.a*p_prime(U(1)))/p.d 1/(-U(1)*p.d)];
%%%%%%%%%%%%%%%%%%%%%%%%%%%%%%%%%%%%%%%%%%%%%%%%%%%%%%%%%
```

```
function out = p_prime(v)

global p


out = -p.gamma * v^(-p.gamma-1);
%%%%%%%%%%%%%%%%%%%%%%%%%%%%%%%%%%%%%%%%%%%%%%%%%%%%%%%

function out = F(x,y)

global p


out =  [y(2,:);(y(1,:)-p.ul(1)+p.a*((y(1,:)^(-p.gamma)...

    -p.ul(1)^(-p.gamma))) - y(2,:)./y(1,:))/p.d];

function out = A(x,lambda,s,p)


v = soln(x,s);
b = 1/v(1);
h = 1-p.a*p.gamma*v(1)^(-p.gamma-1) + v(2)/v(1)^2-lambda/v(1);


out = [0          lambda   1          0;

       0          0        1          0;

       0          0        0          1;

       lambda/p.d lambda/p.d h/p.d        (-b/p.d)];

function out = Aadj(x,lambda,s,p)


v = soln(x,s);
b = 1/v(1);
h = 1-p.a*p.gamma*v(1)^(-p.gamma-1) + v(2)/v(1)^2-lambda/v(1);


out = -[0          lambda   1          0;

        0          0        1          0;

        0          0        0          1;
```

```
      lambda/p.d lambda/p.d h/p.d        (-b/p.d)]';
```

C.4   ANALYTIC_CHOICE

```
function out = analytic_basis(projection,x,preimage,s,p,A,posneg,eps)
% out = analytic_basis(projection,x,preimage,s,p,A,posneg,eps)
%
% Returns an analytic basis at specified infinity using the method of Kato.
%
% Input "projection" is a function handle to the projection function to be
% used, "x" is the numerical value of infinity, "preimage" is the contour
% on which the Evans function is computed, "s" and "p" are structures
% explained in the STABLAB documentation, "A" is a function handle to the
% Evans matrix, "posneg" is 1 or -1 determining which space the
% projection function should return, and "eps" is the tolerance in the
% projection function.

    iterations = size(preimage,2);
    [p_old, Q1] = projection(A(x,preimage(1),s,p),posneg,eps);
    [n,k]=size(Q1);
    out=zeros(n,k,iterations);
    out(:,:,1) = real(Q1);
    for j=2:iterations
        proj = projection(A(x,preimage(j),s,p),posneg,eps);
        %out(:,:,j) = proj * (eye(n) + proj * p_old - p_old * proj) * out(:,:,j-1);
        out(:,:,j) = proj * (eye(n) + 0.5 * p_old * (eye(n)- proj)) * out(:,:,j-1);
        p_old = proj;
     end
```

C.5   CAPA

```
function out=capa(x,y,lambda,s,p,A,n,k,MU)
% out=capa(x,y,lambda,s,p,A,n,k,MU)
%
% Returns the value y'(x) of the first order system y'=(A(x,lambda)-(mu)I)y
%
% Input "x" is the value where y'(x) is evaluated, $y$ is the vector y(x),
% "lambda" is the point in the complex plane where the Evans function is
% evaluated, s,p are structures explained in the STABLAB documentation, "A"
% is a function handle to the Evans matrix, "n" is the dimension of the
% system and "k" is the dimension of the manifold sought, and "MU" is the
% eigenvalue corresponding to the largest or smallest eigenvalue of
% A(\pm \infty,lambda)


out = (A(x,lambda,s,p)-MU*eye(nchoosek(n,k))) * y;
```

C.6   CONTOUR

```
function out=contour(c,s,p,m,e,preimage)
% out=contour(c,s,p,m,e,preimage)
%
% Returns the Evans function output for the given input.
%
% Here c,s,p,m,e are structures described in the introduction of the
% STABLAB documentation. The input preimage is the contour on which the
% Evans function will be computed.

    lbasis=c.basisL(c.proj,c.L,preimage,s,p,c.LA,1,c.epsl);
    rbasis=c.basisR(c.proj,c.R,preimage,s,p,c.RA,-1,c.epsr);
    index=1:(c.ksteps+1):length(preimage);
```

```
    lbasis=lbasis(:,:,index);

    rbasis=rbasis(:,:,index);

    preimage=preimage(index);

    out=zeros(1,length(preimage));


    %parfor j=1:length(index) %Use this for parallel computing
    for j=1:length(index)

        out(j)=c.evans(lbasis(:,:,j),rbasis(:,:,j),preimage(:,j),s,p,m,e);

        j %Take this out for parallel computing

    end
```

C.7 DAVEY

```
function ydot=davey(t,y,lambda,A,s,p,n,k,mu,damping)
% ydot=davey(t,y,lambda,A,s,p,n,k,mu,damping)
%
% Returns the ODE output for the polar method using the method of Davey
%
% Input "t" and "y" are provided by ode45, "A" is a function handle to the
% desired Evans matrix, s,p are structures explained in the STABLAB
% documentation, "n" is the dimension of the system and "k" is the
% dimension of the manifold, "mu" is the rescaling value for increased stability,
% and "damping" is the damping coefficeint.


W = reshape(y(1:k*n,1),n,k);
A_temp=A(t,lambda,s,p);
Winv = pinv(W);
ydot = [reshape((eye(n)-W*Winv)*A_temp*W+damping*W*(eye(k)-W'*W),n*k,1);0];
ydot(end) = (trace(Winv*A_temp*W)-mu)*y(k*n+1,1);
```

C.8 DOUBLE_F

```
function out = double_F(x,y)
% out = double_F(x,y)
%
% Returns the split domain for the ode given in the function F.
%
% Input "x" and "y" are provided by the ode solver. Note that s.rarray
% should be [1,2,...,k] and s.larray should be [k+1,k+2,...,2k]. See
% STABLAB documentation for more inforamtion about the structure s.


global s


out = [(s.R/s.I)*F(x,y(s.rarray,:));(s.L/s.I)*F(x,y(s.larray,:))];
```

C.9 DRURY

```
function ydot=drury(t,y,lambda,A,s,p,n,k,mu,damping)
% ydot=drury(t,y,lambda,A,s,p,n,k,mu,damping)
%
% Returns the ODE output for the polar method using the method of Drury
%
% Input "t" and "y" are provided by ode45, "A" is a function handle to the
% desired Evans matrix, s,p are structures explained in the STABLAB
% documentation, "n" is the dimension of the system and "k" is the
% dimension of the manifold, "mu" is the rescaling value for increased stability,
% and "damping" is the damping coefficeint.


W = reshape(y(1:k*n,1),n,k);
```

```
A_temp=A(t,lambda,s,p);

ydot = [reshape((eye(n)-W*W')*A_temp*W+damping*W*(eye(k)-W'*W),n*k,1);0];

ydot(end) = (trace(W'*A_temp*W)-mu)*y(k*n+1,1);
```

C.10 EVAN

```
function out=evans(yl,yr,lambda,s,p,m,e)
% out=evans(yl,yr,lambda,s,p,m,e)
%
% Returns the evans function output at a given point.
%
% Input "yl" and "yr" are respectively the initializing values on the left
% and right for the desired manifolds, "lambda" is the value in the complex
% plane where the Evans function is evaluated, and s,p,m,e are structures
% explained in the STABLAB documentation.


fun=str2func(e.evans);
out=fun(yl,yr,lambda,s,p,m,e);


%%%%%%%%%%%%%%%%%%%%%%%%%%%%%%%%%%%%%%%%%%%%%%%%%%%%%%%%%%%%%%%%%%%%%%%%%%%%%%
function out=reg_adj_polar(yl,yr,lambda,s,p,m,e)
[omegal,gammal]=manifold_polar(e.Li,orth(yl),lambda,e.LA,s,p,m,e.kl);
[omegar,gammar]=manifold_polar(e.Ri,orth(yr),lambda,e.RA,s,p,m,e.kr);
out=det(orth(yl)'*yl)'*det(orth(yr)'*yr)*gammal'*gammar*det(omegal'*omegar);
%%%%%%%%%%%%%%%%%%%%%%%%%%%%%%%%%%%%%%%%%%%%%%%%%%%%%%%%%%%%%%%%%%%%%%%%%%%%%%
function out=adj_reg_polar(yl,yr,lambda,s,p,m,e)
[omegal,gammal]=manifold_polar(e.Li,orth(yl),lambda,e.LA,s,p,m,e.kl);
[omegar,gammar]=manifold_polar(e.Ri,orth(yr),lambda,e.RA,s,p,m,e.kr);
out=det(orth(yl)'*yl)*det(orth(yr)'*yr)'*gammar'*gammal*det(omegar'*omegal);
%%%%%%%%%%%%%%%%%%%%%%%%%%%%%%%%%%%%%%%%%%%%%%%%%%%%%%%%%%%%%%%%%%%%%%%%%%%%%%%%
```

```
function out=reg_reg_polar(yl,yr,lambda,s,p,m,e)

[omegal,gammal]=manifold_polar(e.Li,orth(yl),lambda,e.LA,s,p,m,e.kl);

[omegar,gammar]=manifold_polar(e.Ri,orth(yr),lambda,e.RA,s,p,m,e.kr);

out=det(orth(yl)'*yl)*det(orth(yr)'*yr)*gammal*gammar*det([omegal omegar]);
% %%%%%%%%%%%%%%%%%%%%%%%%%%%%%%%%%%%%%%%%%%%%%%%%%%%%%%%%%%%%%%%%%%%%%%%%%
```

C.11   MANIFOLD_COMPOUND

```
function out = manifold_compound(x,z,lambda,s,p,m,A,k,pmMU)

% out = manifold_compound(x,z,lambda,s,p,m,A,k,pmMU)

%

% Returns the vector representing the manifold evaluated at x(2).

%

% Input "x" is the interval the manifold is computed on, "z" is the

% initializing vector for the ode solver, "lambda" is the point on the

% complex plane where the Evans function is computed, s,p,m are structures

% explained in the STABLAB documentation, "A" is the function handle to the

% desired Evans matrix, "k" is the dimension of the manifold sought, and

% "pmMU" is 1 or -1 depending on if respectively the growth or decay

% manifold is sought.


[R,D] = eig(A(x(1),lambda,s,p));

[e,mat] = max(real(diag(pmMU*D)));

MU = D(mat,mat);


[X,Z]=ode45(@capa,x,z,m.options,lambda,s,p,A,m.n,k,MU);

out = Z(end,:).';
```

C.12   MANIFOLD_POLAR

```
function [omega,gamma] = manifold_polar(x,y,lambda,A,s,p,m,k)
```

```
% [omega,gamma] = manifold_polar(x,y,lambda,A,s,p,m,k)
%
% Returns "omega", the orthogonal basis for the manifold evaluated at x(2)
% and "gamma" the radial equation evaluated at x(2).
%
% Input "x" is the interval on which the manifold is solved, "y" is the
% initializing vector, "lambda" is the point in the complex plane where the
% Evans function is evaluated, "A" is a function handle to the Evans
% matrix, s,p,m are structures explained in the STABLAB documentation, and k
% is the dimension of the manifold sought.


mu = trace(orth(y)'*A(x(1),lambda,s,p)*orth(y));
[X,Y]=ode45(m.method,[x(1) x(2)],[reshape(y,m.n*k,1);1],m.options,lambda,A,s,p,...
    m.n,k,mu,m.damping);
omega = reshape(Y(end,1:m.n*k).',m.n,k);
gamma = Y(end,m.n*k+1);
```

C.13   PROJECTION1

```
function P = projection1(matrix,posneg,eps)
% P = projection1(matrix,posneg,eps)
%
% Returns a projector P
%
% Input "matrix" is the matrix from which the eigenprojection comes,
% "posneg" is 1,-1, or 0 if the unstable, stable, or center space is
% sought respectively.


[R,D] = eig(matrix);
L = inv(R);
```

```
P = zeros(size(R));


if posneg==1

    index = find(real(diag(D))>0).';

elseif posneg==-1

    index = find(real(diag(D))<0).';

elseif posneg==0

    index = find(abs(real(diag(D)))<eps).';

end


for j=index

    P = P + R(:,j)*L(j,:);

end
```

C.14   PROJECTION2

```
function [P,Q1] = projection2(matrix,posneg,eps)

% [P,Q1] = projection2(matrix,posneg,eps)

%

% Returns a projector P and spanning set Q1 of the invariant subspace

% associated with the given matrix and specified subspace.

%

% Input "matrix" is the matrix from which the eigenprojection comes,

% "posneg" is 1,-1, or 0 if the unstable, stable, or center space is

% sought.


[U,T] = schur(matrix,'complex');

E = ordeig(T);

k = length(find(posneg*real(E)>eps));
```

```
US = ordschur(U,T,posneg*real(E)>eps);

Q1 = US(:,1:k);


[U,T] = schur(-matrix,'complex');

E = ordeig(T);

k = length(find(posneg*real(E)>-eps));

US = ordschur(U,T,posneg*real(E)>-eps);

Q2 = US(:,1:k);


R = [Q1 Q2];

L = inv(R);


P = zeros(size(matrix));

for k=1:size(Q1,2)

    P = P + R(:,k)*L(k,:);

end
```

C.15 RELATIVE_ERROR

```
function out=relative_error(x)

% out=relative_error(x)

%

% Returns max(|x(j+1)-x(j)|/|x(j)|)

%

% Input "x" is a vector whose relative error is sought


out=abs(x(2)-x(1))/abs(x(1));

for j=1:length(x)-1

   out=max(out,abs(x(j+1)-x(j))/abs(x(j)));

end
```

C.16 SEMICIRC

```
function [preimage]=semicirc(circpnts,imagpnts,ksteps,r,spread,zerodist)
% [preimage]=semicirc(circpnts,imagpnts,ksteps,r,spread,zerodist)
%
% Returns a quarter of a semicircle
%
% Input "circpnts" is the number of points on the circle part, "imagpnts"
% is the number of ponits on the imaginary axis, "ksteps" is the number of
% kato steps taken (and are later taken out of the contour), "r" is the
% radius of the semicircle, "spread" is a constant that spreads the points
% on the imaginary axis so that they are more dense near the origin, and
% "zerodist" is how close along the imaginary axis the contour comes to the
% origin.

    p1=(circpnts-1)*ksteps+circpnts;
    p2=(imagpnts-1)*ksteps+imagpnts+ksteps;
    theta = linspace(0,pi/2,p1);
    ln=linspace(r^(1/spread),zerodist^(1/spread),p2).^spread;
    preimage=[r*exp(1i*theta) ln*1i];
```

C.17 SOLN

```
function out=soln(x,s)
% out=soln(x,s)
%
% Returns the solution of bvp problem where the domain was split in half
%
% Input "x" is the value where the solution is evaluated and "s" is a
% stucture described in the STABLAB documenation
```

```
if x<0

    x=s.side*s.I/s.L*x;

    temp=deval(s.sol,x);

    out=temp(s.larray,:);

else

    x=s.side*s.I/s.R*x;

    temp=deval(s.sol,x);

    out=temp(s.rarray,:);

end
```

C.18   WINDING_NUMBER

```
function out=winding_number(w)

% out=winding_number(w)

%

% Returns the winding number of a contour w

%

% Input "w" should be a closed contour not passing through zero.

%

% If f is analytic and nonzero at each point of a simple closed positively

% oriented contour C and is meromorphic inside C, then

% WindingNumber(w)=N0-Np where w=f'(C)./f(C) and N0 and Np are respectively

% the number of zeros and poles of f inscide C (multiplicity included).

%

% The change in the argument between any two points of w should be less than

% Pi for WindingNumber(w) to be accurate.



%Computes the winding number of the contour

out=0;
```

```
for k=1:length(w)-1

    if imag(w(k+1))==0 && real(w(k+1))<0

        kp=pi*sign(imag(w(k)));

    else

        kp=imag(log(w(k+1)/norm(w(k+1))));

    end

    if imag(w(k))==0 && real(w(k))<0

        kc=pi*sign(imag(w(k+1)));

    else

        kc=imag(log(w(k)/norm(w(k))));

    end

    opt1=kp-kc;

    opt2=-(2*pi-abs(opt1))*sign(opt1);

    if min(abs(opt1),abs(opt2))==abs(opt1)

        out=out+opt1;

    else

        out=out+opt2;

    end

end

temp=out/(2*pi);

out=round(temp);
```

References

[1] J. C. Alexander and R. Sachs. Linear instability of solitary waves of a Boussinesq-type equation: a computer assisted computation. *Nonlinear World*, 2(4):471–507, 1995.

[2] J. E. Anderson. *Magnetohydrodynamic shock waves*. MIT Press, 1963.

[3] B. Barker, J. Humpherys, K. Rudd, and K. Zumbrun. Stability of viscous shocks in isentropic gas dynamics. *Comm. Math. Phys.*, 281(1):231–249, 2008.

[4] B. Barker, J. Humpherys, and K. Zumbrun. One-dimensional stability of parallel shock layers in isentropic magnetohydrodynamics. preprint, 2009.

[5] G. K. Batchelor. *An introduction to fluid dynamics*. Cambridge Mathematical Library. Cambridge University Press, Cambridge, paperback edition, 1999.

[6] S. Benzoni-Gavage, D. Serre, and K. Zumbrun. Alternate Evans functions and viscous shock waves. *SIAM J. Math. Anal.*, 32(5):929–962 (electronic), 2001.

[7] T. J. Bridges, G. Derks, and G. Gottwald. Stability and instability of solitary waves of the fifth-order KdV equation: a numerical framework. *Phys. D*, 172(1-4):190–216, 2002.

[8] L. Q. Brin. *Numerical testing of the stability of viscous shock waves*. PhD thesis, Indiana University, Bloomington, 1998.

[9] L. Q. Brin. Numerical testing of the stability of viscous shock waves. *Math. Comp.*, 70(235):1071–1088, 2001.

[10] L. Q. Brin. Numerical testing of the stability of viscous shock waves. *Math. Comp.*, 70(235):1071–1088, 2001.

[11] L. Q. Brin and K. Zumbrun. Analytically varying eigenvectors and the stability of viscous shock waves. *Mat. Contemp.*, 22:19–32, 2002. Seventh Workshop on Partial Differential Equations, Part I (Rio de Janeiro, 2001).

[12] J. C. Bronski. Semiclassical eigenvalue distribution of the zakharov-shabat eigenvalue problem. *Physica D*, 97:376–397, 1996.

[13] H. Cabannes. *Theoretical magnetofluiddynamics*. Academic Press, New York, 1970.

[14] N. Costanzino, J. Humpherys, T. Nguyen, and K. Zumbrun. Spectral stability of noncharacteristic boundary layers of isentropic Navier–Stokes equations. Arch. Ration. Mech. Anal., to appear, 2008.

[15] L. Dieci, R. D. Russell, and E. S. Van Vleck. Unitary Integrators and Applications to Continuous Orthogonalization Techniques. *SIAM J. Numer. Anal.*, 31:261–281, 1994.

[16] J. W. Evans and J. A. Feroe. Traveling waves of infinitely many pulses in nerve equations. *Math. Biosci.*, 37:23–50, 1977.

[17] H. Freistühler and Y. Trakhinin. On the viscous and inviscid stability of magnetohydrodynamic shock waves;. *Physica D: Nonlinear Phenomena*, 237(23):3030–3037, 2008.

[18] J. Goodman. Nonlinear asymptotic stability of viscous shock profiles for conservation laws. *Arch. Rational Mech. Anal.*, 95(4):325–344, 1986.

[19] N. Hale and D. R. Moore. A sixth-order extension to the matlab package bvp4c of j. kierzenka and l. shampine. Technical Report NA-08/04, Oxford University Computing Laboratory, May 2008.

[20] D. Henry. *Geometric theory of semilinear parabolic equations*. Springer-Verlag, Berlin, 1981.

[21] P. Howard and K. Zumbrun. Pointwise estimates and stability for dispersive-diffusive shock waves. *Arch. Ration. Mech. Anal.*, 155(2):85–169, 2000.

[22] J. Humpherys. Spectral energy methods and the stability of shock waves. Dissertation, 2002.

[23] J. Humpherys. On the shock wave spectrum for isentropic gas dynamics with capillarity. *J. Differential Equations*, 246(7):2938–2957, 2009.

[24] J. Humpherys, O. Lafitte, and K. Zumbrun. Stability of viscous shock profiles in the high mach number limit. Comm. Math. Phys, to appear, 2009.

[25] J. Humpherys, G. Lyng, and K. Zumbrun. Multidimensional spectral stability of large-amplitude navier-stokes shocks. In preparation., 2009.

[26] J. Humpherys, G. Lyng, and K. Zumbrun. Spectral stability of ideal-gas shock layers. Arch. Ration. Mech. Anal., to appear, 2009.

[27] J. Humpherys, B. Sandstede, and K. Zumbrun. Efficient computation of analytic bases in Evans function analysis of large systems. *Numer. Math.*, 103(4):631–642, 2006.

[28] J. Humpherys and K. Zumbrun. An efficient shooting algorithm for Evans function calculations in large systems. *Phys. D*, 220(2):116–126, 2006.

[29] C. K. R. T. Jones. Geometric singular perturbation theory. In *Dynamical systems (Montecatini Terme, 1994)*, pages 44–118. Springer, Berlin, 1995.

[30] T. Kato. *Perturbation theory for linear operators*. Berlin Heidelberg New York: Springer, 1985.

[31] S. Kawashima. *Systems of a hyperbolic–parabolic composite type, with applications to the equations of magnetohydrodynamics*. PhD thesis, Kyoto University, 1983.

[32] J. Kierzenka and L. F. Shampine. A BVP solver that controls residual and error. *JNAIAM J. Numer. Anal. Ind. Appl. Math.*, 3(1-2):27–41, 2008.

[33] T.-P. Liu. Nonlinear stability of shock waves for viscous conservation laws. *Mem. Amer. Math. Soc.*, 56(328):v+108, 1985.

[34] T.-P. Liu. Pointwise convergence to shock waves for viscous conservation laws. *Comm. Pure Appl. Math.*, 50(11):1113–1182, 1997.

[35] C. Mascia and K. Zumbrun. Pointwise Green's bounds and stability of relaxation shocks. Preprint, 2000.

[36] C. Mascia and K. Zumbrun. Stability of viscous shock profiles for dissipative symmetric hyperbolic-parabolic systems. Preprint, 2000.

[37] A. Matsumura and K. Nishihara. On the stability of travelling wave solutions of a one-dimensional model system for compressible viscous gas. *Japan J. Appl. Math.*, 2(1):17–25, 1985.

[38] R. L. Pego, P. Smereka, and M. I. Weinstein. Oscillatory instability of traveling waves for a KdV-Burgers equation. *Phys. D*, 67(1-3):45–65, 1993.

[39] R. L. Pego and M. I. Weinstein. Eigenvalues, and instabilities of solitary waves. *Philos. Trans. Roy. Soc. London Ser. A*, 340(1656):47–94, 1992.

[40] E. B. Saff and A. D. Snider. *Fundamentals of Complex Analysis*. Pearson Education, Inc., 2003.

[41] D. H. Sattinger. On the stability of waves of nonlinear parabolic systems. *Advances in Math.*, 22:312–355, 1976.

[42] L. F. Shampine, I. Gladwell, and S. Thompson. *Solving ODEs with MATLAB*. Cambridge University Press, Cambridge, 2003.

[43] A. Szepessy and Z. P. Xin. Nonlinear stability of viscous shock waves. *Arch. Rational Mech. Anal.*, 122(1):53–103, 1993.

[44] K. Zumbrun. Numerical error analysis for evans function computations: a numerical gap lemma, centered-coordinate methods, and the unreasonable effctiveness of continuous orthogonalization. Preprint, 2009.

[45] K. Zumbrun. Numerical error analysis for evans function computations: a numerical gap lemma, centered-coordinate methods, and the unreasonable effectiveness of continuous orthogonalization, 2009.

[46] K. Zumbrun and P. Howard. Pointwise semigroup methods and stability of viscous shock waves. *Indiana Univ. Math. J.*, 47(3):741–871, 1998.